# Response Linearization in Electro-Optic Modulators

by

Peter Omondi Orondo

B.Sc., Massachusetts Institute of Technology (1995)

Submitted to the Department of Electrical Engineering and Computer Science in Partial Fulfillment of the Requirements for the Degree of Master of Engineering in Electrical Engineering and Computer Science at the Massachusetts Institute of Technology

February 1997



Author _____

Department of Electrical Engineering and Computer Science
January 1997

Certified by _____

Cardinal Warde,
Professor of Electrical Engineering.
Thesis Supervisor.

Certified by _____

Dr. Brent Little,
Research Scientist.
Thesis Supervisor

Accepted by _____

Arthur C. Smith,
Professor of Electrical Engineering
Chairman, Department Committee on Graduate Students

# *Dedication*

This thesis is dedicated to my family; my father for being the guiding light in my life for all these years, my mom for the nurturing care without which nothing is possible, and my brothers and sisters for providing inspirational motivation, example and innumerable assistance towards achieving my goals.

Uduto agoyonu erokamano.

# *Acknowledgments*

I owe a debt of gratitude to Prof. Warde for providing the funding without which this thesis would not have been possible, Dr. Brent Little for his motivation, guidance and endless patience, and Vern Shrauger for his much needed assistance in securing equipment and many experimental hints. Thank you all.

I would also like to thank Tom MacNamara for valuable experimental insight, my friends Dennis Ouma, John Gachora, Victor Owuor, and all others for their comradeship.

# Response Linearization in Electro-Optic Modulators

by

Peter Omondi Orondo

Submitted to the
Department of Electrical Engineering and Computer Science

January 15 1997

In Partial Fulfillment of the Requirements for the Degree of Master of Engineering in Electrical Engineering and Computer Science

## ABSTRACT

Linearity of the electro-optic modulator used in an optical communications link is one of the most critical factors that affects the performance of the entire line. Two highly optimized linearized modulator designs are presented. We present a feedback linearization technique and demonstrate that using a simple and robust closed loop feedback system, limited only by electrical component characteristics such as frequency response and slew rate, we can achieve arbitrary reduction in distortion products of an electro-optic modulator. Furthermore, it is shown that feedback can be used with other linearization techniques to correct for errors introduced by fabrication uncertainties.

Thesis Supervisor: Cardinal Warde
Title: Professor of Electrical Engineering.

Thesis Supervisor: Dr. Brent Little
Title: Visiting Research Scientist, Research Laboratory of Electronics.

# *Table of Contents*

# *List of figures*

# *List of Equations*

*Chapter 1*

# Introduction and Background

## Introduction

Long-haul transmission of video signals over fiber-optic cables offers a superior alternative to the long chains of repeater amplifiers that are used in current cable television transmission systems. Besides gains in available bandwidth, there is a clear advantage to using fiber-optic cables due to their reliability, low loss, and linearity. Furthermore an analog line uses bandwidth conservatively and ensures compatibility with existing equipment. Indeed the vestigial sideband amplitude modulated (VSB-AM) fiber-optic transmission systems have received a lot of attention recently, especially due to the advances in optical modulator technology[1].

The performance of an optical-fiber link is closely related to that of the modulator used to implement it[2]. Important characteristics of the modulator include frequency response, sensitivity and linearity. Linearity in optical modulators refers to the response of the optical output intensity as a function of RF drive voltage. In general, linearity is difficult to achieve in optical modulators because modulation arises from an induced interference of waves, an inherently non-linear process. The primary goal of this work is to make the response of such a modulator linear.

The rest of this chapter reviews basic modulation theory. The criteria used to measure linearity are discussed and linearization techniques in current literature are presented. Chapter 2 reviews waveguide theory and presents a design of a perturbation 3-waveguide optical modulator. An apodized tapered-coupler

modulator design is also analyzed and theoretical results presented. Chapter 3 discusses the dynamics of a feedback-assisted linearized modulator and theoretical predictions of how feedback might be used to overcome fabrication uncertainties, while Chapter 4 provides the experimental results and analysis of a prototypical modulator which has been linearized using electrical feedback. Chapter 5 concludes the discussion and offers some possible areas of further work.

## Summary of Original Work Presented

This thesis presents the following original result.

1. A feedback-assisted modulator has been theoretically analyzed and a useful expression for a customizable design derived. We show how closed-loop feedback can be used to improve the linearity of modulators designed by other conventional means reported in literature. Furthermore, we show that a device with less non-linearity to begin with requires a lower gain feedback loop and hence is faster than one which is not. This suggests a useful symbiosis between feedback linearization and other prevalent techniques as an effective solution that either one alone.

# Optical Modulation.

## Overview

The electro-optic effect refers to change in the refractive index of a material as a result of application of electric field. This refractive index change can be described by the equation

$$\Delta\left(\frac{1}{n_r^2}\right) = r^l E + s^q E^2$$

Equation 1: General refractive index change with applied E-field.

$r^l$ is the linear electro-optic coefficient and $s^q$ is the quadratic electro-optic coefficient. When $r^l$ is very large compared to $s^q$ we have the linear electro-optic effect also known as Pockel's effect. If $s^q$ is large and makes the quadratic term dominant then the corresponding electro-optic effect is called the Kerr effect. In general anisotropic medium, $r^l$ and $s^q$ depend on the direction of the applied electric field in the medium and are described by tensors[3].

From the foregoing, it is evident that the application of an electric field will cause the propagation constant of the waves in that medium to change. In particular, if an electric field is applied to one arm of a directional coupler, waves propagating in that arm will experience a phase delay relative to those in the second arm with no field applied. When the two waves recombine vectorially, the amplitude of the resulting wave will depend on the relative phase delay between them. We thus achieve amplitude modulation. When the modulation is due to an externally applied voltage, we have external modulation. Direct modulation is achieved by controlling the actual laser generating mechanisms directly at the source. In this work, we will concentrate on externally modulation. There is extensive literature on direct modulation, for example Cox et al[4].

# Conventional Electro-Optic Modulation

## Linearization Criteria

One scheme of external modulation is to employ a CW laser and an external electro-optic integrated optical intensity modulator[2] as shown in Figure 1 (b). A conventional interferometric modulator (Figure 1 (a)) consists of an input waveguide that splits into two arms and recombines interferometrically. The intensity transmission of the device varies sinusoidally with the phase difference between optical fields in the two arms, Figure 2. The device has been biased in quadrature i.e. to the linear portion of the sine curve to achieve the best possible linearity. However, this response is highly non-linear and thus has a very limited linear dynamic range. Consider an input of unity amplitude applied to this quadrature biased device. The output intensity will be given by

$$I_{out} = \sin(x) = x - \frac{x^3}{3!} + \frac{x^5}{5!} \ldots$$

Equation 2: Output intensity of interferometric modulator expanded in Taylor series.

after expanding the equation around $x = 0$ and $x$ is the relative phase difference discussed above. If we define the distortion level as

$$Distortion(dB) = 10 * \log\left(\frac{cubic\_term}{linear\_term}\right)$$

Equation 3: Intermodulation distortion (dB).

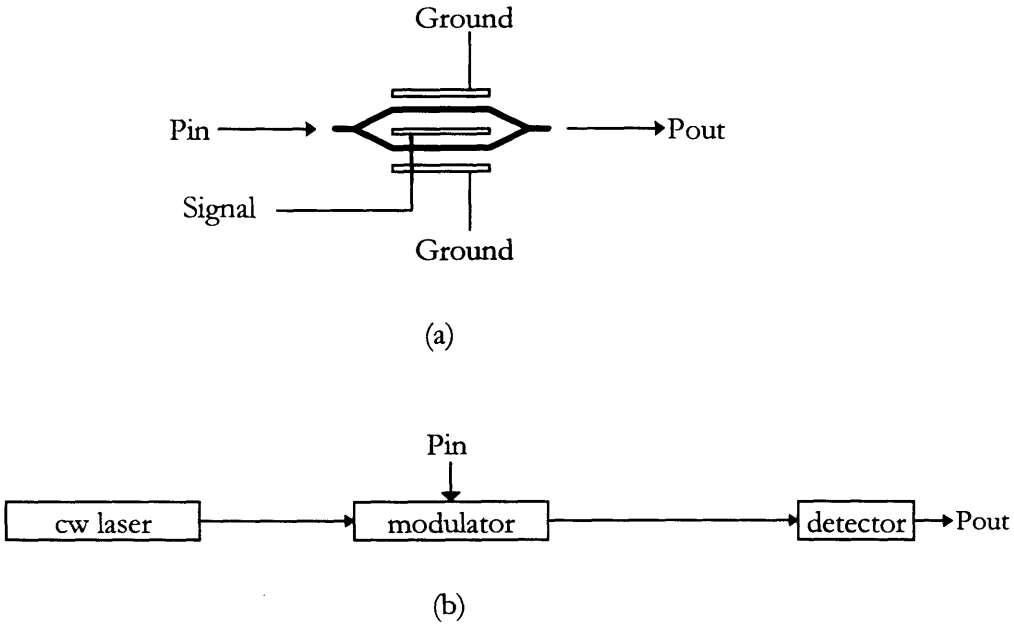


Figure 1: (a) Integrated-optical interferometric intensity modulator. A signal (voltage) applied to the electrodes modulates the optical transmission. (b) Externally modulated analog fiber-optic link[2].

and use the current VSB-AM standards of -50dB distortion level[1], we find that the above quadrature biased interferometer of Figure 2 only has a linear dynamic range (LDR) of

$$LDR = \sqrt{6*10^{-5}} = 8*10^{-4} radians$$

This low LDR makes the device unsuitable for CATV applications because only extremely weak signals can be transmitted without producing unacceptable distortion in the output signal. When many cable channels are transmitted using an optical modulator, the distortion produced because of modulator non-linearity is referred to as inter-modulation distortion (IMD) and is essentially calculated as outlined above. In a multi-channel transmission system, the non-linearity further places a limit on the number of channels that can be transmitted because IMD increases roughly with the number of channels. Even though the second order

IMD can be filtered out, CATV systems operate over wide a bandwidth as to render such filtering impossible[5].

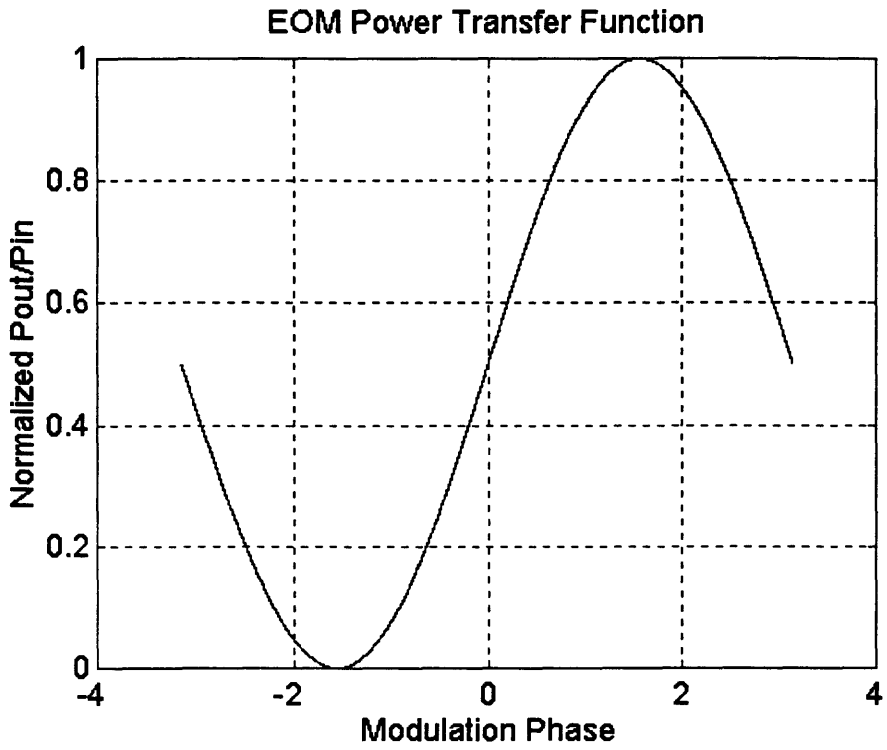


Figure 2: Optical transmission of an interferometric modulator biased at half power point[2]

# Review of Current Literature

Several authors[5] [6] [7] [8] [9] have suggested ways to linearize the response of an electro-optic modulator (EOM). Many of these schemes are based on the fact that the transfer function of an EOM biased in quadrature can be expressed as an odd Taylor series. The authors then choose design parameters such that the third order Taylor series term is eliminated or balanced against the fifth order term.

Liu and co-workers[5] analyze a device formed from a cascade of Y-branch that splits the optical power equally into two channels, Mach-Zehnder

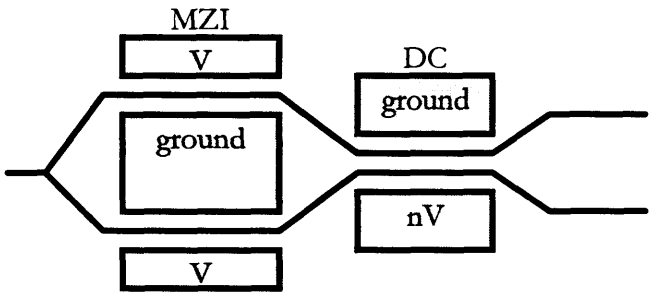


Figure 3: The schematic of the device proposed in Ref 5. Both the Mach-Zehnder and the directional coupler are modulated. The modulation signals are of opposite polarity.

Interferometer (MZI) working as a phase shifter and a Directional Coupler (DC) of nominal coupling constant-length equal to $\kappa * L = \frac{\pi}{4}$, Figure 3. The Mach-Zehnder interferometer has the following response:

$$I = I_o \cos^2(\Delta\beta L)$$

Equation 4: Response of Mach-Zehnder interferometer.

where $2.\Delta\beta L$ is the phase difference between the two arms, $L$ is the length of the interferometer and $I_o$ is the input optical power. The directional coupler output and input optical power are related by

$$I = I_o \frac{\kappa^2}{\kappa^2 + \Delta\beta^2} \sin^2(\sqrt{\kappa^2 + \Delta\beta^2}\, L)$$

Equation 5: Response of a directional coupler.

where $\kappa$ is the coupling constant, L is the length, and $\Delta\beta = (\beta_1 - \beta_2)/2$. $\beta_1$ and $\beta_2$ are the propagation constants in the two waveguides. There are two sets of electrodes as shown in Figure 3 and the signal applied to the MZI is linearly related to that applied to the DC, $\eta = V_1 / V_2$. The second harmonic and second IMD can be zeroed by biasing the MZI and the directional coupler at their half power points, and by optimizing $\{\kappa L, \eta\}$, the authors show that the third order harmonic and 3rd IMD can be minimized.

Skeie and Johnson[6] analyze a device quite similar to that of Liu's shown in Figure 3 except that the second modulating drive is eliminated and the additional degree of freedom gained by cascading two such devices. By carefully tuning the bias points of the two Mach-Zehnder interferometers and the input signal distribution, they achieve cancellation of the 2nd and 3rd derivatives (and hence the 2nd and 3rd order distortions terms and IMD). Additionally, cascading the devices allows for fabrication uncertainties to be balanced out.

Lam and Tangonan[7] use a similar Taylor series solution to optimize the linearity of the device shown in Figure 4. It consists of a tandem of two directional couplers. The first of these DCs is driven by an external voltage ($\Delta\beta_1 L_1 \neq 0$) and has length $L_1$ and coupling constant $\kappa_1$. The second has a length $L_2$ coupling constant $\kappa_2$ and $\Delta\beta L_2 = 0$. For a specific set of the parameters $\{\kappa_1 L_1, \kappa_2 L_2, \Delta\beta_1 L_1\}$, the third order IMD is eliminated.

Djuspjõbacka[10] uses a dual parallel Mach-Zehnder modulator scheme to achieve reduction in 3rd order IMD. By optimizing the ratio of input optical power in the two MZI arms and various biasing elements, he is able to achieve total cancellation of between 3rd and 5th order distortion terms. Refer to Djuspjõbacka's paper[10] for detailed description of the modulator. However, to ensure quadrature operation in all active elements of his device, the modulator

suffers a very high overhead from a complicated voltage arrangement. Other dual parallel schemes are also discussed in Korotky's article[8].

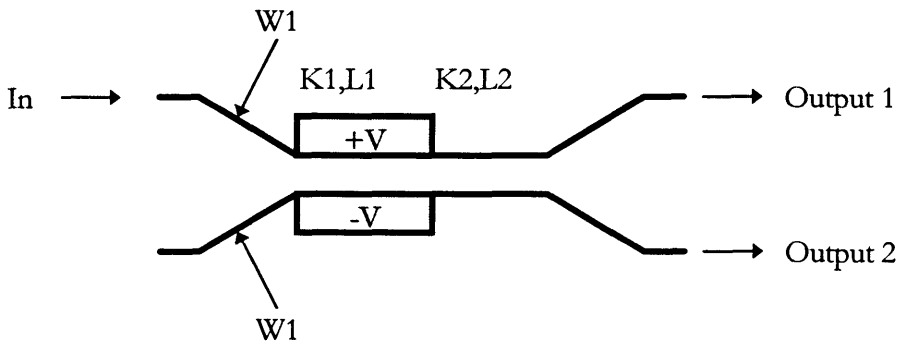


Figure 4: A tandem of two-directional coupler system[7]. The first directional coupler has waveguides of unequal widths, which sets a finite static phase difference $\Delta\beta_0$.

Burns[9] reports a linearized device that is an extension of Skeie and Johnson's[6] but includes three MZI-DC sections instead. An extra adjustable parameter in the last DC allows for the removal of the fifth as well as the third order Taylor series terms in a device much simpler than the comparable one by Djuspjõbacka[10]. Using a three-tone signal, Burns achieves excellent reduction in distortion terms. Each MZI section is driven by a signal in the ratio 1:-1:1 and, as he points out, even higher order terms can be eliminated by additional cascade sections. However, the device is rather long from the several cascades.

Other than the parametrized solutions discussed above, several authors have investigated methods that apply carefully chosen optical input or modulation signal in order to achieve near-linear modulation. Johnson and Roussell[11,12] use a carefully chosen combination of TE/TM to excite a modulator that supports both polarization modes. Because TE and TM waves have slightly different

propagation constants, the authors can adjust the modulator bias such that the transfer functions of the two polarization modes have slopes of opposite signs, Figure 5. The modulator 3rd order non-linearity can be substantially reduced vis-à-vis the linear term by controlling the relative power in each mode.

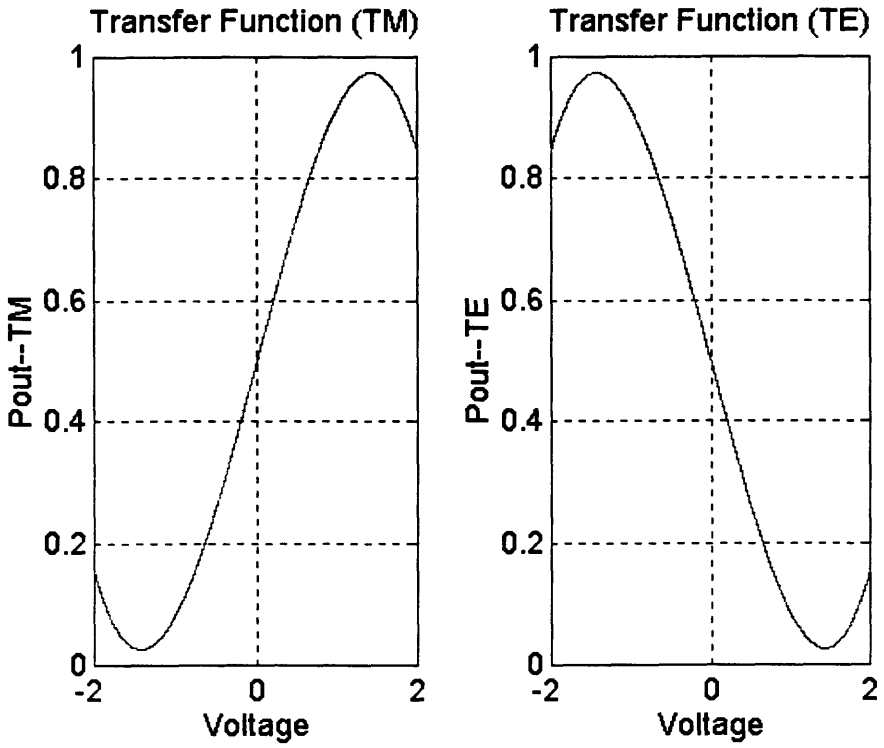


Figure 5: Ideal phase bias condition of an interferometric modulator with the use of polarization mixing technique. Pout_TE and Pout_TM designate the TE and TM modulator output power, respectively, as a function of applied voltage[12].

Childs and et al[13] present a pre-distortion technique that significantly reduces the dominant distortion in an both directly and externally modulated devices. The block diagram of the pre-distortion arrangement is shown in Figure 6 below:

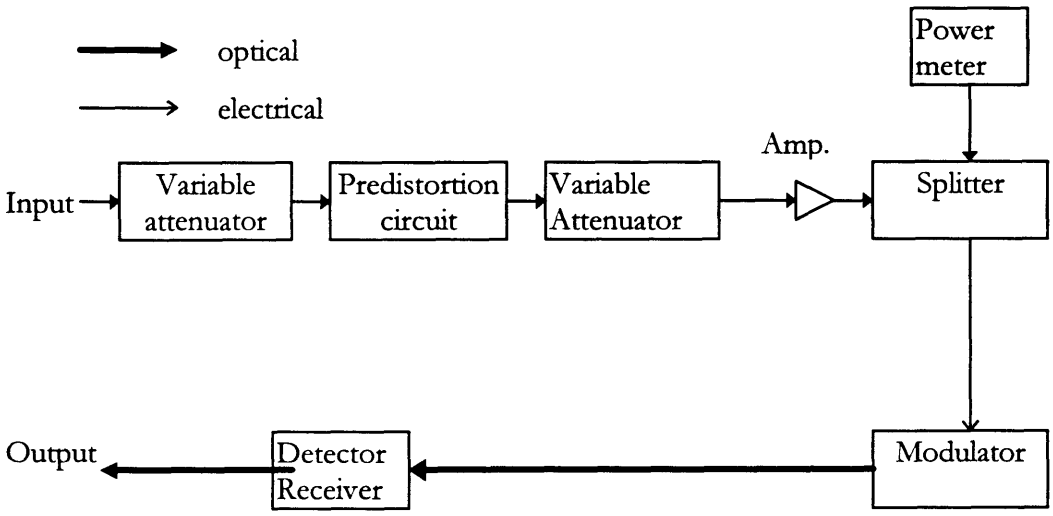


Figure 6: Block diagram of pre-distortion apparatus[13].

The pre-distortion circuit consists of a non-linear element which generates distortion products equal in amplitude but opposite in phase with the distortion products produced by the modulator. A quadrature-biased Mach-Zehnder modulator, for example, would require an element that generates 3rd order distortion without significant 2nd order non-linearities. This is normally implemented using a balanced arrangement of Schottky diodes with exponential transfer functions. However due to parasitic reactances in the components of the

pre-distortion circuit, the distortion characteristics will vary with frequency. Also, for accurate reduction in distortion, the circuitry required will be complicated.

## Summary

The linearization techniques presented thus far mostly rely on very accurate control of fabrication parameters like propagation constants, $\kappa$, coupling length and constant biases[5,6,7,8,9]. Very linearized device solutions are possible but fabrication tolerances are normally very tight even in designs that attempt to balance out fabrication uncertainties as Skeie and Johnson's[6]. Furthermore, the devices sometimes end up with very complicated drive voltage arrangement as in Djuspjõbacka's[10]. Other schemes like Johnson and Roussell's[11,12] require an exacting mixing of TE/TM components, also very difficult to achieve in a practical system. Pre-distortion linearization[13] suffers from it's fundamental dependence on frequency. A simpler, robust method that doesn't suffer from these limitations is thus required.

*Chapter 2*

# Synthesization of Linearized Electro-Optic Waveguide Modulators

## Introduction

Electro-optic modulators are usually made out of waveguide structures and transitions or junctions. Primarily these are the Mach-Zehnder interferometers (MZIs), directional couplers (DCs) and some branching structure, e.g. Y-branch. Both MZI and DC consist of waveguides fabricated by diffusing titanium into an electro-optic material like Lithium Niobate[14]. Depending on the design, one or both of MZIs and DCs may be modulated and there could be multiple MZI-DC sections. MZIs rely on electromagnetic wave interference for operation as described in Chapter 1. Directional couplers use evanescent coupling to transfer electromagnetic power from one waveguide to another. By controlling device length and shape, we can control the characteristics of the output optical power as described in the following sections.

## Modulator Components

### The Mach-Zehnder Interferometer

The Mach-Zehnder interferometer is shown in Figure 7. It consists of a Y-branch that splits incoming optical power into two arms then recombines them in another Y-branch[15]. With a gradual enough Y-branch taper, the power splitting can be accomplished without too much

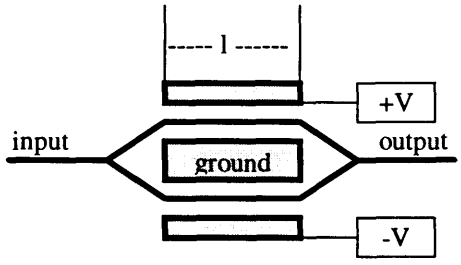


Figure 7: Mach-Zehnder Interferometer

power loss. This type of branching is referred to a slow or adiabatic transition[16]. The basic operation of the MZI is quite simple. When there is no phase difference in both arms (or the difference is a multiple of $2\pi$), then the waves in the two arms add constructively in the output arm and all power (assuming no waveguide material loss) appears in the output arm. If the phase difference is $\pi$, the waves interfere destructively and all the power is radiated into the substrate[15]. Since the phase difference in the two arms is controlled by the applied voltage, we can control the output power and hence achieve modulation.

# The Directional Coupler

## Basic Waveguide Theory

The directional coupler consists of two waveguides fabricated in close proximity. In each waveguide, optical waves travel as optical modes. Modes are spatial distributions of optical energy[14] or, equivalently, a mode can be described mathematically as a solution to Maxwell's wave equation

$$\nabla^2 E(r,t) = \frac{n^2(r)}{c^2}\frac{\partial^2 E(r,t)}{\partial t^2}.$$

Equation 6: Maxwell's equation.

$E$ is the electric field vector, $r$ is a position vector, $n(r)$ is the index of refraction profile and $c$ is the speed of light in a vacuum[14]. For monochromatic waves, i.e. waves that can be thought of as consisting of approximately of a single frequency, we can express the electric field vector as

$$E(r,t) = E(r)e^{j\omega t}$$

Equation 7: Electric field vector expression.

where $\omega$ is the frequency. Substituting (7) into (6), we get

$$\nabla^2 E(r) + k^2 n^2(r) E(r) = 0,$$

Equation 8: Helmholtz equation.

for $k \equiv \frac{\omega}{c}$.

Consider a simple planar waveguide, Figure 8. The $\{z, y\}$ extent is considered infinite for mathematical ease. For $z$-propagating plane waves, we can express the electric field as

$$E(r) = E(x,y)e^{-j\beta^* z}.$$

Equation 9: Expression of generalized optical field.

$\beta$ is the propagation constant in the z-direction. Substituting in Equation 8 we get

$$\frac{\partial^2 E(x,y)}{\partial x^2} + \frac{\partial^2 E(x,y)}{\partial y^2} + [k^2 n^2(r) - \beta^2]E(x,y) = 0.$$

Equation 10: Differential equation describing modes of a slab waveguide.

The solutions to Equation 10 are either sinusoidal or exponential depending on whether $(k^2 n^2(r) - \beta^2)$, is greater than or less than zero and are well known for many other waveguide structures[14, 17]. There exist various approximations also, e.g. Kogelnik's effective index method [18]. For the planar waveguide of Figure 8,

we can divide the waveguide into the logical three layers in the x-direction and solve Equation 10 for each region. From the foregoing, the possible solutions of Equation 10 and hence the modes of the planar waveguide structure, are shown in Figure 9.

A necessary condition for guiding in the middle layer is that $kn_2 > kn_3 > kn_1$. For $\beta > kn_2$, $E(x)$ is exponential in all regions and is not a physically realizable because it implies the field increases unboundedly in regions 1 and 3 (case [a]). Cases [b] and [c] correspond to the two guided modes of the structure. [b] is the lowest guided mode, also called the symmetric guided mode. [c] is the second lowest or the anti-symmetric mode. [d] is the substrate radiation mode and continually loses energy from the waveguiding region 2 to the substrate, region 3, via evanescent coupling. While not useful for signal transmission, this mode can be exploited to design couplers as described below. [e] represents an unguided mode.

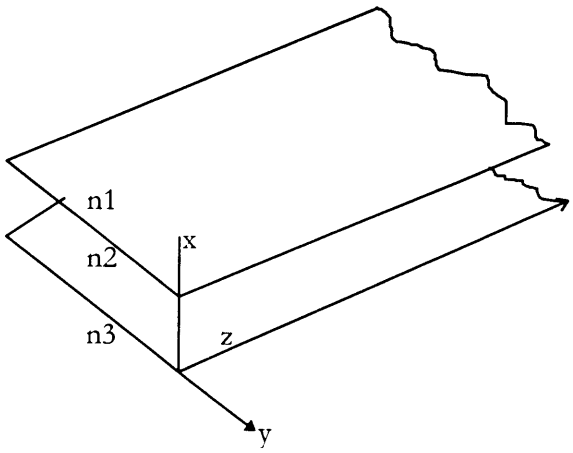


Figure 8: A three-layer planar waveguide structure[14].

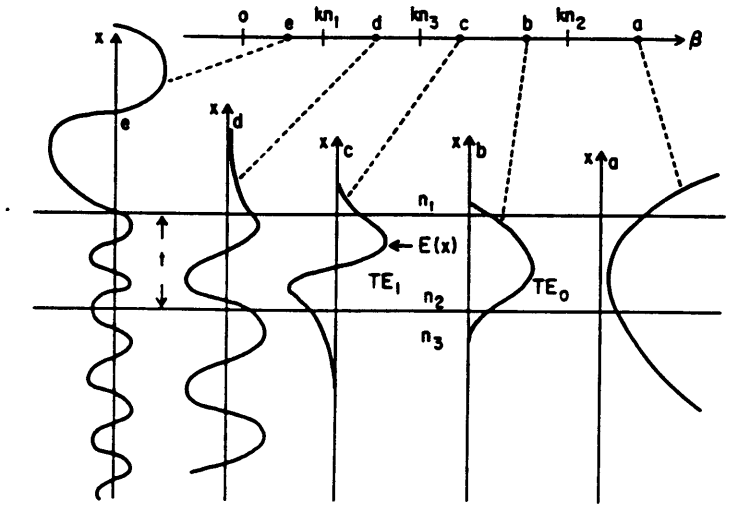


Figure 9: Possible modes of a planar waveguide.
After Hunsperger[14]

## Mode Coupling

The guided symmetric and anti-symmetric modes [b] and [c] in Figure 9 are also referred to as the normal modes of the three layer structure. The symmetric mode will be denoted by $\psi_i$ and the anti-symmetric mode by $\psi_j$. Suppose two waveguides that can each support a single symmetric mode and are sufficiently close together such that their optical fields overlap. The two waveguides are then said to be coupled because optical power can be transferred between them via their evanescent fields---the tail end of optical power distribution that extends beyond the guiding region in cases [b] and [c] in Figure 9.

## Coupled Mode Theory

When two waveguides are in close proximity, we can further define the normal modes of the coupled waveguide structure, also denoted by $\psi_i$ and $\psi_j$ for symmetric and anti-symmetric modes, respectively. Normal modes, by definition, are only defined when the waveguide structure is constant with length[19]. Following Tamir[16], we then employ the concept of locally normal mode which is defined for some position $z_o$, Figure 10. Local normal modes are then considered to evolve as they propagate in a geometrically varying structure. As before, structures whose geometric variation in length occurs so slowly that no power is transferred between local normal modes are said to be slow or adiabatic. Structures whose geometric transition occurs in such a way that maximum power is transferred between local normal modes are said to be fast or abrupt[19].

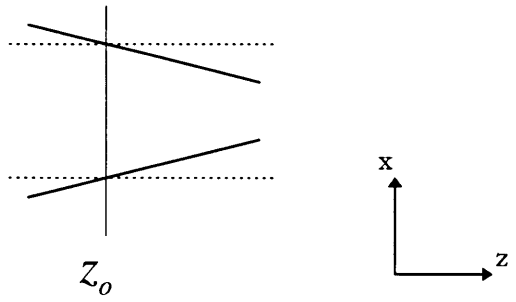


Figure 10: To define a local normal mode, the slowly varying waveguide structure (solid line) is replaced at $z_o$ by a structure constant with z (dashed line) and the normal mode solutions at $z_o$ are obtained[14].

For two waveguides *a* and *b* separated by a distance D, the coupling strength between them is measured by the coupling constant

$$\kappa = Ce^{-\gamma D}$$

Equation 11: Coupling strength between two waveguides.

where $C$ is a constant and $\gamma$ is the transverse component of the propagation constant of the electric field in the region between the waveguides[16]. Following Hardy and Streifer[20], and Marcatili[21], we have ignored any differences between $\kappa_{ab}$, the coupling coefficient from guide $a$ to guide $b$, and $\kappa_{ba}$ and further take $\kappa$ to be real. Phase mismatch or asynchronism is the difference in propagation constants of the individual guides at large separation, $\Delta\beta = \beta_a - \beta_b$.

To describe the power transfer between the coupled waveguides, we can use coupled mode theory[16]. We assume that each waveguide mode retains the transverse shape of the uncoupled modes $\phi_a$ or $\phi_b$ but the coupled mode acquires a mode amplitude that will vary with position along the waveguide. Let $a$ and $b$ denote the coupled-mode amplitudes, then the coupled-mode equations (slow/adiabatic form) can be shown to be[15]

$$\frac{da}{dz} + j\beta_a a + j\kappa^* b = 0,$$

$$\frac{db}{dz} + j\beta_b b + j\kappa^* a = 0.$$

Equation 12: Two guide coupled-mode equations.

where the amplitude coefficients vary with the direction of propagation. Solutions to Equation 12 are well known[16].

Alternatively, we can use an approximate coupled-mode representation for the normal modes of the coupled-waveguide system[19]. In this approach, local normal modes are assumed to propagate in the coupled-waveguide system without a change in amplitude. The local normal modes, $\psi_i$ , $\psi_j$, are formed out of a linear combination of the uncoupled modes $\phi_a$ and $\phi_b$

$$\psi_i = d\phi_a + e\phi_b$$

$$\psi_j = -e\phi_a + d\phi_b$$

Equation 13: Local normal modes expressed as a linear combination of uncoupled modes.

where normalization requires that $d^2 + e^2 = 1$ and $\int \psi_i \psi_j^* dx = \{^{0, i \neq j}_{1, i = j}$ .

# Synthesization of Linearized Modulators

## Introduction

Using the local normal mode representation outlined above, we can now design linearized modulators by exploiting the underlying physics of mode propagation. Two design solutions are presented here. One utilizes a 3-waveguide system and optimizes for coupling constant-length product as well as constant phase shift. The other uses filter design techniques to produce an apodized coupling profile. These devices are considerably shorter and have much simpler drive arrangements than similar one proposed in literature.

## 3-Waveguide Device

We considered a 3-waveguide device. Our approach involved starting out with a simple 2-waveguide 3-dB coupler then adding a third "perturbation" waveguide which added additional degree of freedom to remove higher order non-linear terms. First, we will solve a linearized two-waveguide coupler consisting of two 3-dB coupler sections and a Mach-Zehnder section acting as a phase shifter.

## 2-Waveguide Device.

The two-waveguide device is shown in Figure 11. Optical power fed into the bottom waveguide couples into the top guide in two coupling sections. We will derive the output power of the device by assuming that the coupling sections are adiabatic. First, we make the following simplifying assumptions:

1. The coupling sections are each 3dB couplers, i.e. each guide couples half its power to the adjacent guide. This implies that the coupling constant-length product for the two sections is the same, $\kappa_1 l_1 = \kappa_2 l_2$.
2. The guides have the same propagation constant, i.e., $\delta = \beta_1 - \beta_2$, also known as detuning, is zero.

Considering just one 3dB coupler section, the coupled mode equations are:

$$\frac{da_1(z)}{dz} = -j\beta_1 a_1(z) - j\kappa a_2(z)$$

$$\frac{da_2(z)}{dz} = -j\beta_2 a_2(z) - j\kappa a_1(z)$$

Equation 14: Two guide coupled-mode equations (specific).

where $a_1, a_2$ are the coupled-mode amplitudes. To solve these coupled equations, assume there exist solutions (eigenmodes) of the following form[15]:

$$a_1(z) = a_1 e^{-j\beta z}$$

$$a_2(z) = a_2 e^{-j\beta z}$$

Equation 15: General coupled-mode solution expressions (two guides).

for some $a_1$, $a_2$. Substituting Equation 15 into Equation 14 and setting $\beta_1 = \beta_2 = \beta_0$, we get

$$\overline{\overline{A}}\,\bar{a} = 0$$

Equation 16: Eigenvalue equation for two guide coupler.

for $\overline{\overline{A}} = \begin{bmatrix} \beta - \beta_o & -\kappa \\ -\kappa & \beta - \beta_o \end{bmatrix}$ and $\bar{a} = \begin{bmatrix} a_1 \\ a_2 \end{bmatrix}$.

Equation 16 has non-trivial solutions only when the determinant of $\overline{\overline{A}}$ vanishes. Using this fact, we solve for the eigenvalues of coupled-waveguide, $\beta$:

$$\beta = \beta_o \pm \kappa.$$

Equation 17: Eigenvalues for two-guide coupled mode equations.

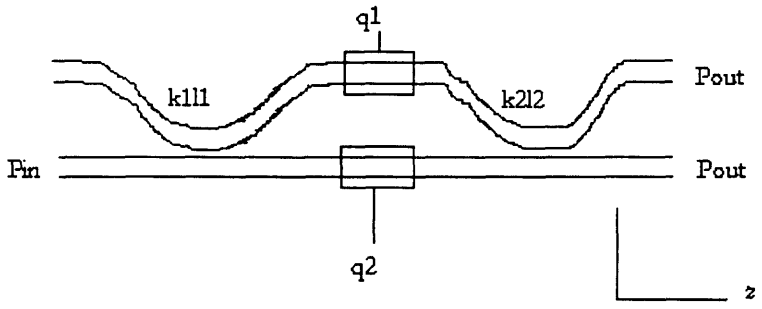


Figure 11: 2-waveguide device made from two 3dB couplers and Mach-Zehnder interferometer acting as a phase shifter.

This is an eigenvalue problem. We can easily solve for the eigenvectors corresponding to these eigenvalues then piece together the full solution using as yet undetermined constants $c_1$ and $c_2$. After some algebra, the two solutions are:

$$\begin{bmatrix} a_1(z) \\ a_2(z) \end{bmatrix} = c_1 \begin{bmatrix} 1 \\ 1 \end{bmatrix} e^{-j(\beta_o+\kappa)z} + c_2 \begin{bmatrix} 1 \\ -1 \end{bmatrix} e^{-j(\beta_o-\kappa)z}$$

Equation 18: General solutions for eigenvector equation (two-guide).

These solutions can then be substituted into the original coupled-mode equations, Equation 14, and for the initial conditions $a_1(z)|_{z=0} = a_1(0)$ and $a_2(z)|_{z=0} = a_2(0)$, we can solve for $c_1$ and $c_2$ in terms of the known terms:

$$c_1 = \tfrac{1}{2}[a_1(0) + a_2(0)]$$

$$c_2 = \tfrac{1}{2}[a_1(0) - a_2(0)]$$

Equation 19: Solutions for constants in Eqn 18.

The full solution is obtained by plugging Equation 19 into Equation 18. After this has been done, we end up with a simple and cascadable solution that expresses the output of the 2-guide coupler in terms of the input coupled-mode amplitudes:

$$\begin{bmatrix} a_1(z) \\ a_2(z\_ \end{bmatrix} = e^{-j\beta_o z} \begin{bmatrix} \cos(\kappa z) & -j\sin(\kappa z) \\ -j\sin(\kappa z) & \cos(\kappa z) \end{bmatrix} \begin{bmatrix} a_1(0) \\ a_2(0) \end{bmatrix}$$

Equation 20: Full solution of two guide coupler in terms of initial conditions.

For an input $\begin{bmatrix} 0 \\ 1 \end{bmatrix}$, i.e., a normalized optical power is fed into the bottom waveguide only, in the case of a 3dB coupler, we want the output power to be $P_{out} = \frac{1}{2}$ in both waveguides, assuming no loss. Solving,

$$P_{out}^1 = \sin^2(\kappa z) = \frac{1}{2}$$

$$P_{out}^2 = \cos^2(\kappa z) = \frac{1}{2}$$

Equation 21: Output power condition for 3dB coupler.

or

$$\kappa z = \frac{\pi}{4}.$$

Equation 22: Coupling constant-length product for 3dB coupler.

To get the power output of the whole device, we cascade Equation 20 with the transfer function of the Mach-Zehnder section. Since the modes are not coupled at the Mach-Zehnder, the transfer function is particularly simple,

$$\overline{\overline{A}}_{MZI} = \begin{bmatrix} e^{-j\phi_1} & 0 \\ 0 & e^{-j\phi_2} \end{bmatrix}$$

Equation 23: Transfer matrix for a Mach-Zehnder.

where

$$\phi_1 = \phi_{o1} + \phi$$

$$\phi_2 = \phi_{o2} + \phi$$

Equation 24: Phases in the two Mach-Zehnder arms in Eqn 2-19.

for some fixed biases, $\phi_{o1}$, $\phi_{o2}$ and a signal part, $\phi$. Cascading the three portions, we get the full input-output relationship for the simple two-waveguide modulator:

$$\begin{bmatrix} a_1(z) \\ a_2(z\_ \end{bmatrix} = e^{-j2\beta_o z} \begin{bmatrix} \cos(\kappa z) & -j\sin(\kappa z) \\ -j\sin(\kappa z) & \cos(\kappa z) \end{bmatrix} \begin{bmatrix} e^{-j\phi_1} & 0 \\ 0 & e^{-j\phi_2} \end{bmatrix} \begin{bmatrix} \cos(\kappa z) & -j\sin(\kappa z) \\ -j\sin(\kappa z) & \cos(\kappa z) \end{bmatrix} \begin{bmatrix} a_1(0) \\ a_2(0) \end{bmatrix}$$

Equation 25: Full cascade solution for DC-MZI-DC two waveguide modulator.

For $\kappa z = \frac{\pi}{4}$, solutions exist that have only odd-harmonics. One of these solutions involves driving the two MZI arms with opposite voltages (signals) and setting biases as follows:

$$\phi_{o1} = 0,$$

$$\phi_{o2} = \frac{\pi}{2}.$$

Equation 26: Phase relationships in Mach-Zehnder for quadrature biasing.

This solution is plotted in Figure 12.

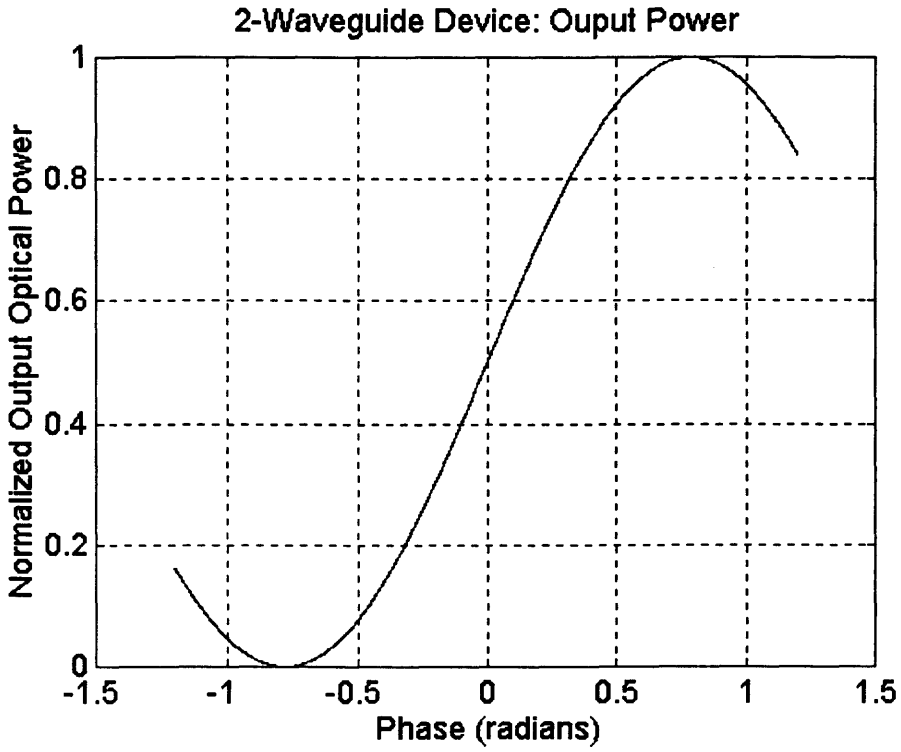


Figure 12: Transfer function of the 2-waveguide modulator. Quadrature biasing ensures zero even harmonics.

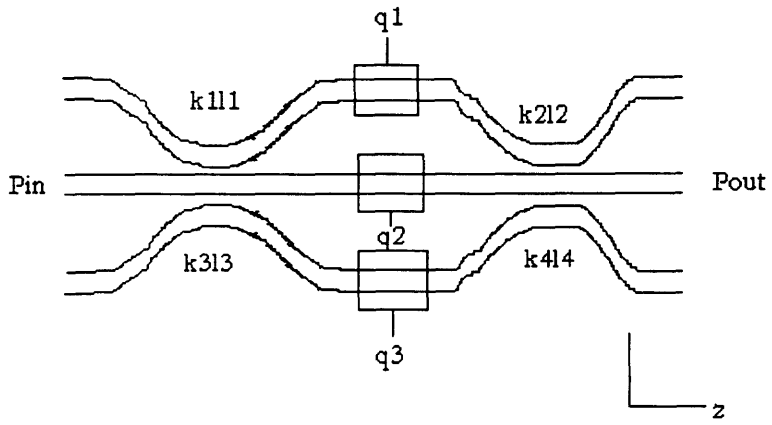


Figure 13: 3-waveguide modulator. The bottom guide has additional degrees of freedom in the constant phase factor q3 and the two coupling sections.

## Removing the Odd Harmonics

To remove the odd harmonics also, we add a third "perturbation guide" as shown in Figure 13. The Mach-Zehnder section is driven by a constant bias $q3 = \phi_0$ and only the middle waveguide is excited.

Following essentially the eigenvalue method outlined for the 2-waveguide device above, we can derive the input-output relationship of the 3-waveguide. The coupled-mode equations for the coupled-mode amplitudes become

$$\frac{da_1(z)}{dz} = -j\beta_1 a_1(z) - j\kappa_a a_2(z)$$

$$\frac{da_2(z)}{dz} = -j\beta_2 a_2(z) - j\kappa_a a_1(z) - j\kappa_b a_3(z)$$

$$\frac{da_3(z)}{dz} = -j\beta_3 a_3(z) - j\kappa_b a_2(z)$$

Equation 27: Coupled-mode equations for 3-waveguide coupler.

where $\beta_i$, $i = 1,2,3$ are the respective guide propagation constants, $\kappa_{12} = \kappa_{21} = \kappa_a$ is the coupling constant from guide 1 to guide 2 and vice-versa, and $\kappa_b$ correspondingly for guides 2 and 3. It is assumed that there is coupling only between adjacent guides. Solving for the coupled-mode amplitudes as before and cascading the results together with the Mach-Zehnder input-output relationship, we arrive at the following solution:

$$\begin{bmatrix} a_1(z) \\ a_2(z) \\ a_3(z) \end{bmatrix} = \overline{\overline{M_{DC}}}(\delta_2, \delta_4)\overline{\overline{M_{MZI}}}(\phi, \phi_o)\overline{\overline{M_{DC}}}(\delta_1, \delta_3)\begin{bmatrix} a_1(0) \\ a_2(0) \\ a_3(0) \end{bmatrix}$$

Equation 28: Full solution for 3-guide modulator.

where $\overline{\overline{M_{DC}}}(\delta_2, \delta_4)$ is the input-output relationship of a 3-guide coupler assuming coupling between adjacent guides only, $\delta_2 = k_2 l_2$ is the coupling constant-length product between the 1st and 2nd guide, and $\delta_4 = k_4 l_4$ the coupling constant-length product between the 2nd and 3rd guide as depicted in Figure 13. To get the expression for $\overline{\overline{M_{DC}}}(\delta_2, \delta_4)$, we follow the same procedure as for the two-guide device previously outlined (Equations 15 to 20). The result is

$$\overline{\overline{M_{DC}}}(x, y) = \begin{bmatrix} \frac{1}{x^2+y^2}[y^2 + x^2\cos(\bar{k}z)] & \frac{-jx}{\sqrt{x^2+y^2}}\sin(\bar{k}z) & \frac{-xy}{x^2+y^2}[1-\cos(\bar{k}z)] \\ \frac{-jx}{\sqrt{x^2+y^2}}\sin(\bar{k}z) & \cos(\bar{k}z) & \frac{-jy}{\sqrt{x^2+y^2}}\sin(\bar{k}z) \\ \frac{-xy}{x^2+y^2}[1-\cos(\bar{k}z)] & \frac{-jy}{\sqrt{x^2+y^2}}\sin(\bar{k}z) & \frac{1}{x^2+y^2}[x^2 + y^2\cos(\bar{k}z)] \end{bmatrix}$$

Equation 29: Expression for transfer matrix for 3-guide coupler.

where $\bar{k} = \sqrt{x^2 + y^2}$.

$\overline{\overline{M_{MZI}}}(\phi, \phi_o)$ is the input-output relationship of the Mach-Zehnder.

For any specified initial conditions, Equation 28 is a function of the parameters $\{\kappa_3 l_3, \kappa_4 l_4, \phi_0\}$ only. An optimal solution that minimizes higher order harmonics

can then be found. See Appendix A for the optimization routines used. For an input/initial condition $\begin{bmatrix} a_1(z) \\ a_2(z) \\ a_3(z) \end{bmatrix} = \begin{bmatrix} 0 \\ 1 \\ 0 \end{bmatrix}$, the output power on the 2nd guide is found to be:

$$P_{out}^2 = .4999999998 - .1972936469 * \sin(2 * v).*\sin(-1.153879772 - v) + .1972936469 * \cos(2 * v).*\cos(-1.153879772 - v) + .08737726311 * \sin(-1.153879772 - v) - .01812637914 * \sin(2 * v);$$

Equation 30: Numerical solution for 3-guide modulator.

The results are listed below in terms of the size of the harmonics in dB below fundamental (dBf), defined as $dBf = 10 * \log_{10}\left[\frac{harmonic\_term}{fundamental\_term}\right]$:

1. $\kappa_3 l_3 = 1.495251000$
2. $\kappa_4 l_4 = 1.988625661$
3. $\phi_0 = -1.153879772$
4. 2nd Harmonic = -89.4dBf
5. 3rd Harmonic=-92.6dBf
6. 4th Harmonic=-100.8dBf
7. 5th Harmonic=-14.8dBf

The result is plotted in Figure 14.

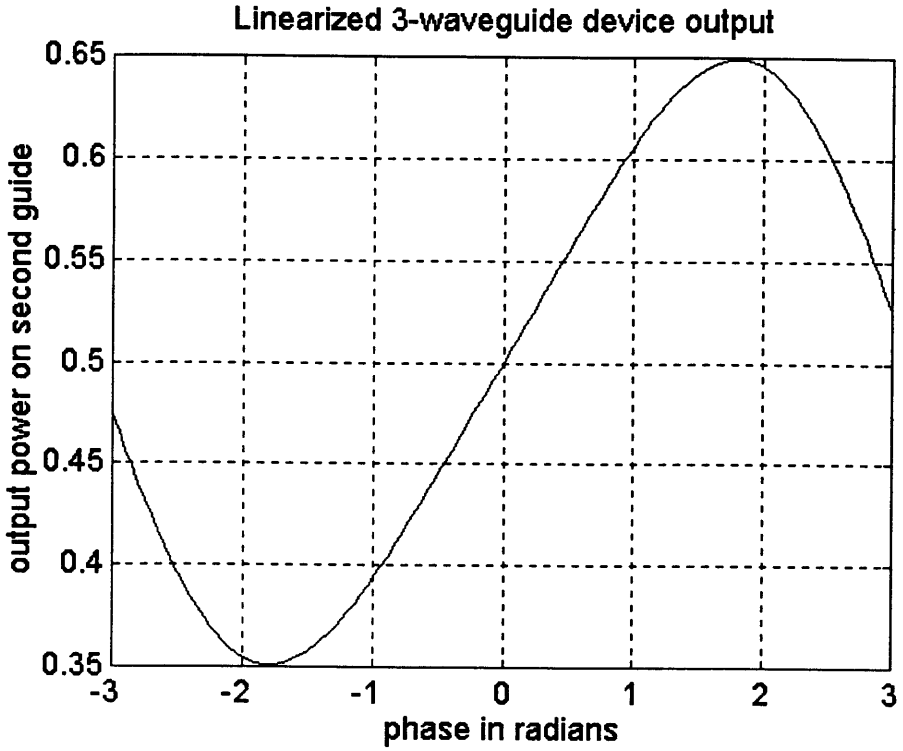


Figure 14: Linearized 3-waveguide output power. Up to the 4th harmonic has been reduced to virtually zero.

# Fabrication Considerations

The solution just presented is very numerically unstable. Any small deviation from the exact solutions leads to a significant increase in harmonic terms. For example, rounding off the values of $\{\kappa_3 l_3, \kappa_4 l_4, \phi_0\}$ above to 5 decimal places to account for any fabrication errors leads to an increase of the 2nd order harmonic term from -89.4 to -51.0dBf and the 3rd order harmonic from -92.6 to 52.7dBf. 4th order harmonic term increases from -100.8 to -61.8dBf. As we show in the next chapter, we can use electrical feedback to correct for these fabrication uncertainties.

# The Apodized Waveguide Modulator

## Introduction

If one had unlimited fabrication accuracy, then in principle one could design a perfectly linearized optical modulator through a judicious choice of device shape. The current fabrication limits do not permit the realization of such devices with the required sub -50 dB harmonic distortion. Nonetheless, improvements can be realized over the typical MZ or directional coupler configurations.

Such improved devices are worthwhile for their incorporation into the feedback modulation scheme discussed in Chapter 3, because a modulator with improved static linearity leads to a more relaxed requirement in terms of gain for the feedback differential amplifier.

In this section we highlight a method to solve for the required shape of directional couplers that lead to the fulfillment of -60 dB harmonic distortion. The solutions specify how the propagation constants of each waveguide and their mutual coupling coefficient should vary along the device length. The approach is based on variational optimization[22], as well the adiabatic principle[23].

## Adiabatic Couplers

First we describe the adiabatic type of device, which serves as the base structure before optimization. As previously noted, two waveguides which are placed in close proximity will exchange power, Figure 15. If an optical signal is launched into one arm of the coupler at the input end, then the division of power at the output can be controlled by adjusting the shape and length of the coupler and also by adjusting the asynchronism between the two waveguides.

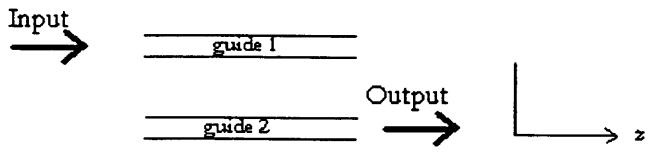


Figure 15: Parallel waveguide coupler.

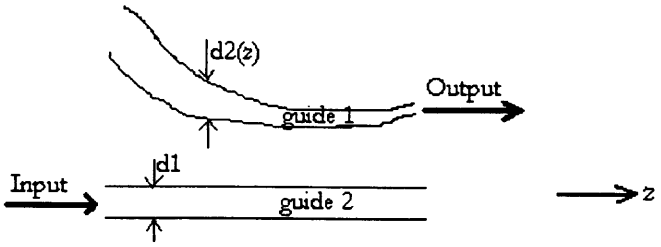


Figure 16: Adiabatic coupler.

The typical parallel coupler, in which the two waveguides remain equidistant, and for which the total length is selected to be the so called beat length, exhibits a response similar to that of a $\sin c^2(V)$, where $V$ is proportional to the voltage, Figure 17. One may operate the device at the half power points $A$ and $B$ as shown in Figure 17. However, the linearity is limited. It can be seen in Figure 17 that the response is not monotonic. If the voltage is increased or decreased sufficiently around the bias points, A or B, the output power eventually oscillates. An improvement can be realized if the power level as a function of voltage can be made to vary monotonically. This is possible using the concept of adiabatic

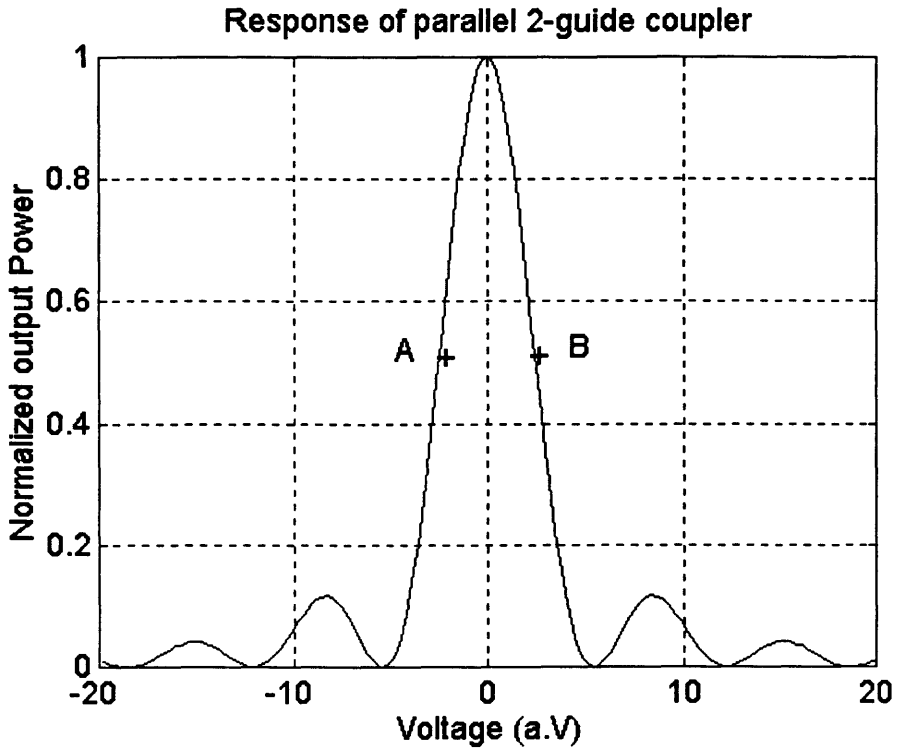


Figure 17: Response of a parallel 2-guide directional coupler.

power exchange as highlighted in Little's article[23] and applied to wavelength filters.

Consider the tapered coupler depicted in Figure 16. At both ends of the device the waveguides are well separated, and hence the coupling strength is zero. The two waveguides are gradually brought into close proximity from the ends towards the center, where they are strongly interacting. The coupling strength as a function of position along the device would in this case look somewhat Gaussian, Figure 18. This type of modification of the interaction strength is known as apodization.

In addition to the longitudinal dependence of the coupling strength, the synchronism between the waveguides is also smoothly varying with position.

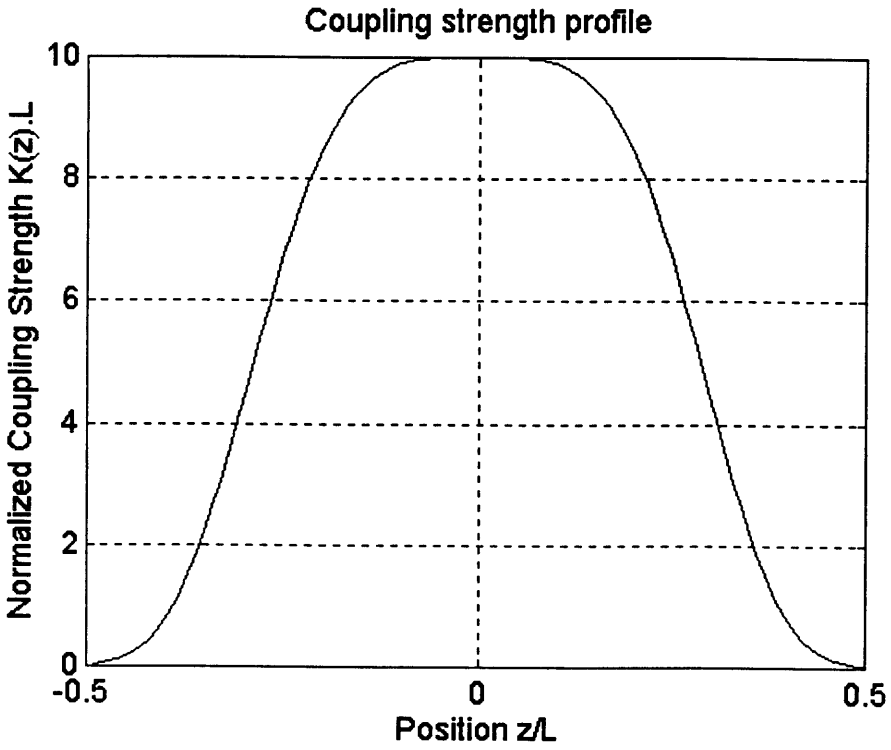


Figure 18: A super-Gaussian coupling profile

The synchronism can be modified by varying the index of one or both waveguides, or by varying the dimensions of the waveguides, such as the width. In Figure 16, one waveguide (guide 1) remains uniform along its length, while the second waveguide (guide 2), has a taper. The taper is such that the width of guide 2 is larger than that of guide 1 at the input end, and narrower at the output end. The propagation constant in guide 2 is thus made to monotonically decrease from the input end to the output end along the device, Figure 19.

If the tapers or apodization in both coupling coefficient and synchronism are sufficiently slow, adiabatic power transfer occurs[23]. This means that power launched into guide 1 exits guide 2, regardless of the exact details of the structure. Further, if the index of one of the guides is made to vary due to an applied voltage, the power at the output will either increase or decrease

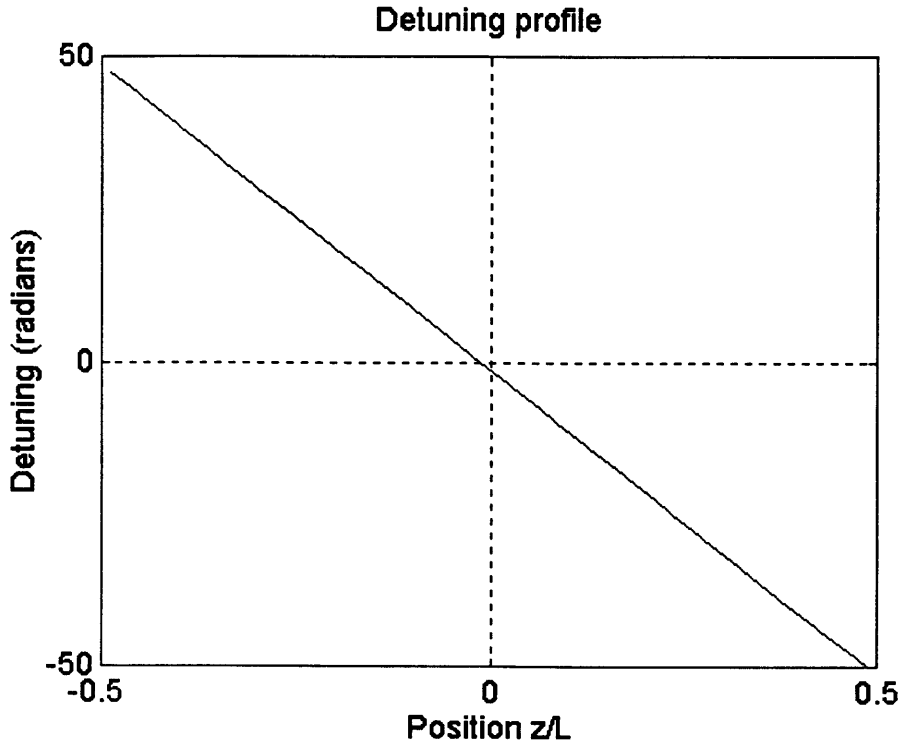


Figure 19: Detuning profile in apodized coupler.

monotonically, as shown in Figure 20. On this modified structure, the half power points $A$ or $B$ serve as modulator bias points.

Using the foregoing adiabatic structure, the response is further improved using variational optimization[22].

## Coupler Optimization

The modulation response of the foregoing adiabatic directional couplers can be further enhanced by manipulating the device shape (coupling strength and synchronism) on a finer scale. The objective of this section is to show that this can be achieved in theory, and how to go about accomplishing the design goal in practice. An unlimited number of structures may be found which satisfy our

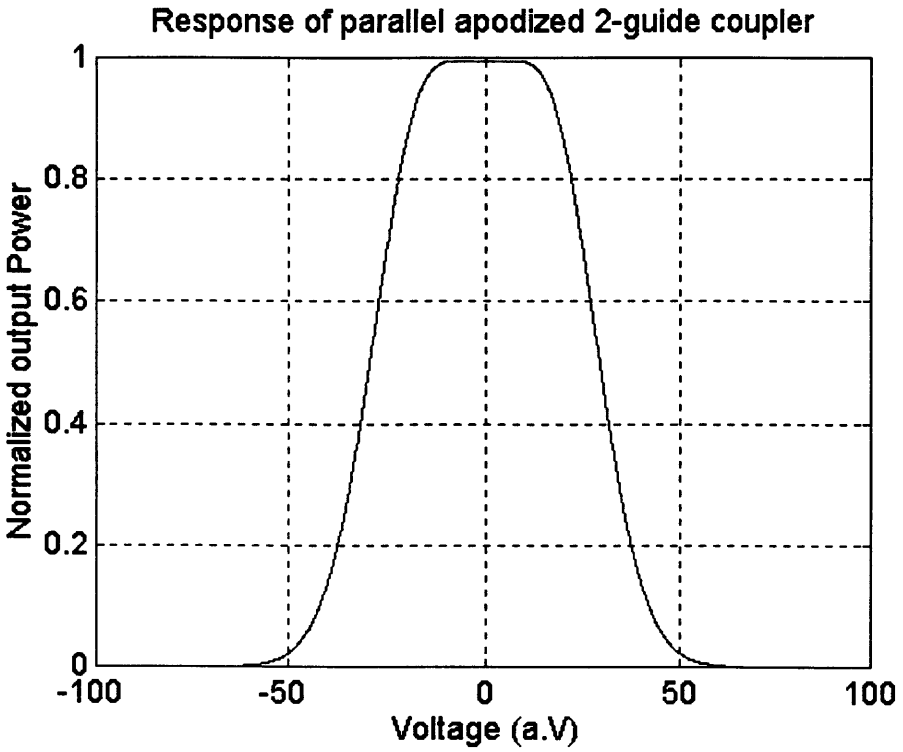


Figure 20: Response of the apodized coupler.

design criteria of sub -60 dB harmonic distortion, and thus only a single characteristic example is shown.

For numerical evaluation, the coupler is subdivided into a large number of uniform sections and over each section the power transfer characteristics are evaluated by the coupled-mode equations, Equation 12. Expressed generally, the slow form of coupled-mode equations, Equation 12, become[22]

$$\frac{dA_1}{dz} = -j\kappa(z)e^{jA\Delta\beta z}A_2$$

$$\frac{dA_2}{dz} = -j\kappa(z)e^{-jA\Delta\beta z}A_1$$

Equation 31: Generalized coupled-mode equations.

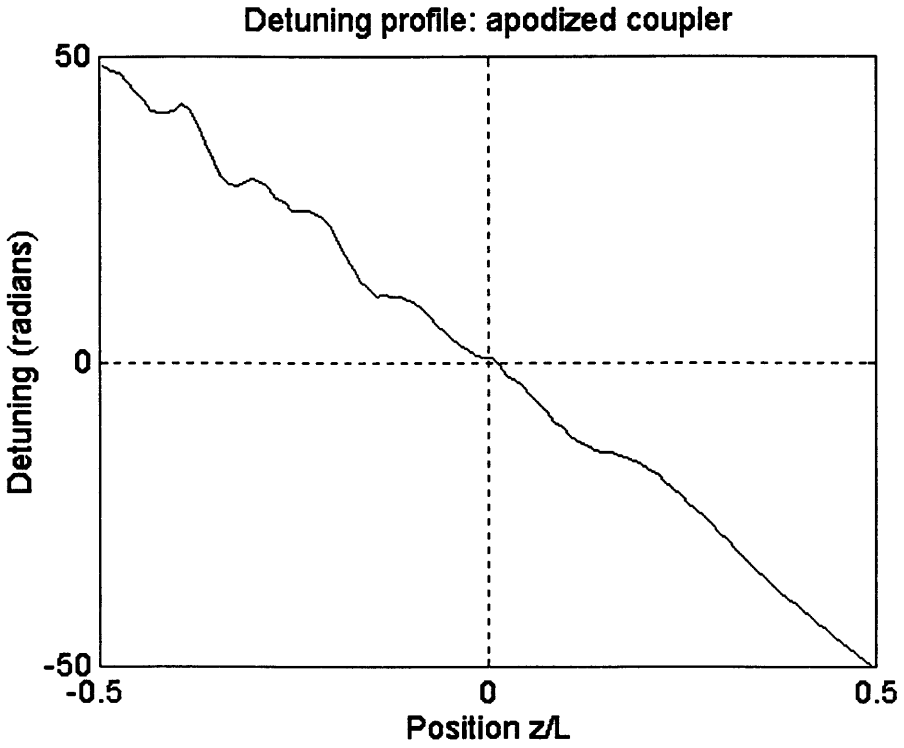


Figure 21: Detuning profile for the 2-guide apodized coupler.

where as before $\Delta\beta = \beta_1 - \beta_2$ is phase mismatch or detuning for evanescently coupled guides. $\kappa(z)$ is the $z$-dependent coupling constant while $A_1$ and $A_2$ represent appropriately defined mode amplitudes. In terms of guide effective indices, $n_{eff1}$ and $n_{eff2}$, detuning can be expressed as

$$\Delta\beta = k_o(n_{eff1} - n_{eff2})L$$

Equation 32: Detuning in terms of indices of refraction.

where $k_o$ is the free space propagation constant of the optical input and $L$ is the device length. These effective indexes are governed by the detailed structure of the waveguides and by their actual refractive index. The effective

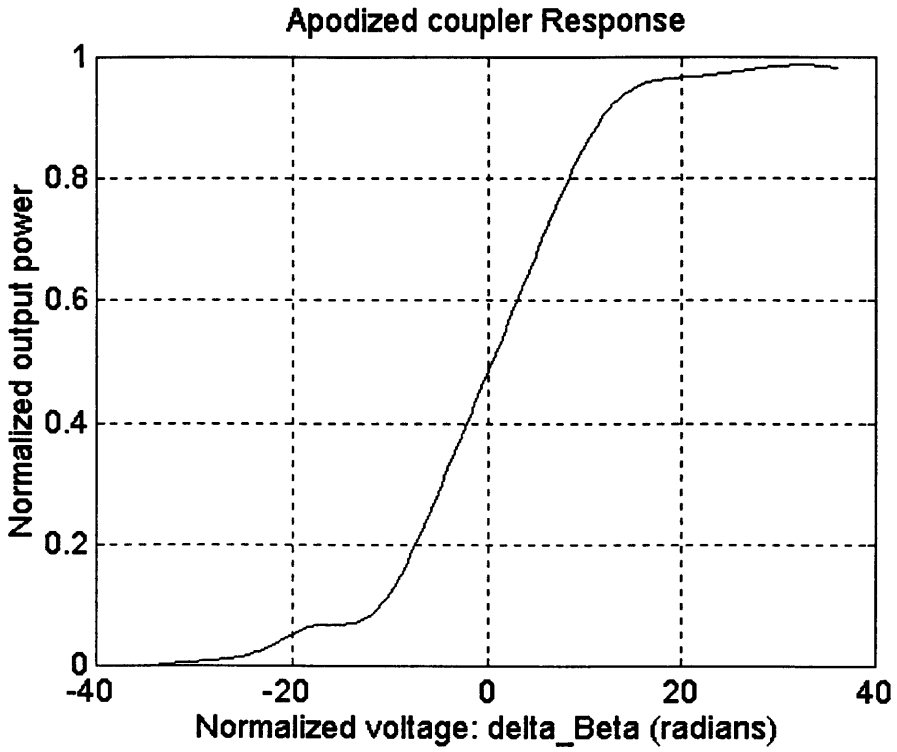


Figure 22: Response function for apodized 2-guide coupler.

indexes can also vary due to the modulating electric field, and hence we can write in general

$$(n_{eff1} - n_{eff2}) = \alpha(V - V_o)$$

Equation 33: General expression of effective index change in terms of applied voltage

where $V$ is the signal voltage, $V_o$ is a bias voltage, and $\alpha$ is a proportionality constant.

For our example, we choose the coupling strength profile of the device to be fixed with the apodization shape

$$K(z) = 10e^{-100(z/L)^4}$$

Equation 34: Coupling strength profile (super-Gaussian).

Equation 34 is a super-Gaussian, Figure 18. $z$ is the position along the coupler with $z = 0$ as the center, and $L$ is the physical device length. The modulator is optimized by varying the synchronism along the device. In order to perform the linearization, a suitable bias point near the half power point is selected. Around this point the second through sixth order derivatives are minimized.
An example of the foregoing optimization scheme is shown in Figures 18 through 23.

Figure 18 shows the coupling strength profile, which was pre-selected to be super-Gaussian, while Figure 21 shows the required detuning between the two waveguides along the coupler length, which has been evaluated by optimization. Figure 22 shows the modulator response, while Figure 23 indicates the level of harmonic distortion as a function of modulation depth. The curves in Figure 23 where evaluated by applying a sinusoidal modulation to the modulator and calculating the third harmonic amplitude relative to the fundamental at the output. For comparison, the harmonic distortion of the uniform directional coupler of Figure 15, is also plotted.

## Summary

This chapter has shown that, in principle, it is possible to design devices with excellent linearity through a proper choice of device parameters. However because of limitations in fabrication accuracy, computed device parameters cannot be fabricated precisely enough for -50dB distortion level required for operational devices. The next chapter will present the feedback approach that eliminates some of these fabrication difficulties.

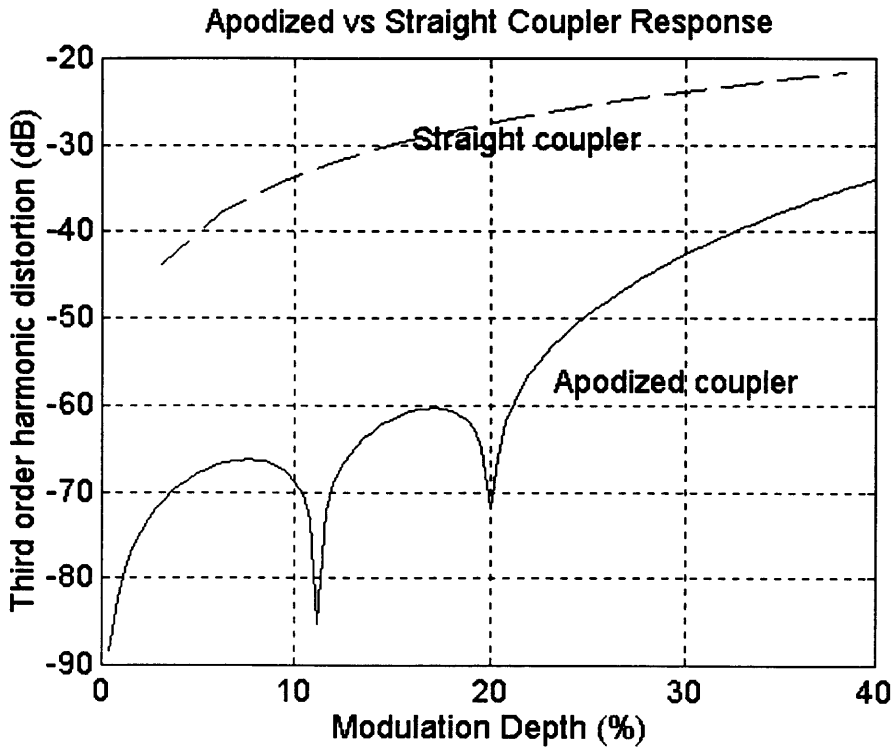


Figure 23: Third harmonic distortion for optimized vs. straight coupler.

*Chapter 3*

# Modeling the Feedback-Assisted Modulator

## Basic Feedback Control Theory

Feedback control is a well established concept in control systems. The basic idea involves using the deviation of a system output from its desired value to form a corrective signal which is then applied to the input. The system refers to a physical 'plant' or machine we desire to control. Usually, there also is some control function which is used to compensate for undesired plant behavior[24].

An example of a feedback system is shown below, Figure 24. The desired output is $r(t)$ while the actual plant output is $c(t)$. The error signal, $e(t) = r(t) - c(t)$, drives the compensating element $G_c(s)$ which produces a corrective input signal $m(t)$, which is then applied to the plant, $G_p(s)$. $s$ is a system parameter representing frequency and denotes that, in general, the response of the plant as well as that of the compensating element are dependent on the frequency of the input signal.

The system transfer function is the ratio between the output signal $c(t)$, and the input, $r(t)$. In an ideal system, this transfer function should be unity. In real systems, it is rarely so and in fact depends in the input frequency, amongst other parameters. If the plant is linear, it is possible to derive a closed-form expression for the system's transfer function, $H(s)$. If the plant is non-linear, then the transfer function can only be derived implicitly.

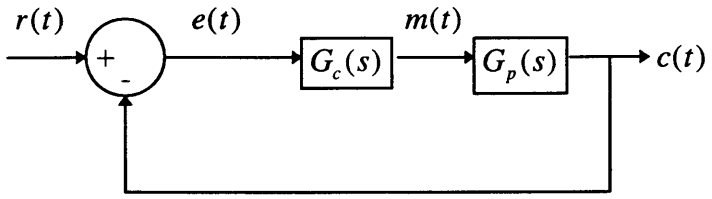


Figure 24: A typical block diagram for feedback control[24]

For the moment, let's assume that the plant is linear. The transfer function of the system in Figure 24 is given by

$$H(s) = \frac{C(s)}{R(s)} = \frac{G_c(s)G_p(s)}{1 + G_c(s)G_p(s)}$$

Equation 35: Transfer function of a linear system.

and provides the starting point for further analysis of the plant's behavior. See Koppel[24], for example.

Intuitively, from Figure 24, and with our stated goal to make the output signal $c(t)$ follow the desired value $r(t)$, we can immediately see that a well designed compensating element $G_c(s)$ will drive the plant in such a way as to make the output tend towards $r(t)$ as much as possible. Clearly one criterion for choosing $G_c(s)$ is to make it as large as possible. In that case, if $G_c(s)G_p(s) >> 1$, then $\frac{C(s)}{R(s)} \to 1$, our desired linear result. A large $G_c(s)$, combined with the adder can be realized with an opamp or high gain differential amplifier, thus our motivation for a differential amplifier feedback configuration.

# Feedback-Assisted Modulator

## Introduction

A generalized electro-optic modulator has a non-linear transfer function. The transfer function in this case relates the input-output optical powers, i.e.,

$$H(s) = \frac{I_{out}}{I_{in}}$$

Equation 36: Optical Input-output transfer function.

where $I_{out}$ is the modulated optical output and thus depends on the modulating signal and bias. $I_{in}$ is a constant optical field (laser beam) and is usually normalized to 1. We will now show mathematically how a closed loop with high gain can linearize the output of a modulator.

## Adding Closed Loop Feedback

Consider the modulator in Figure 25. Some of the detected power is tapped, amplified $\beta$ times and fed back to the modulator via a differential amplifier, with differential amplification $\alpha$. From Figure 25, we see that the differential amplifier will drive the modulator at whatever level is required to equalize its two input terminals, precisely the behavior we seek in a linearized modulator. In other words, the differential amplifier, given appropriate gain, will linearize the output of the modulator.

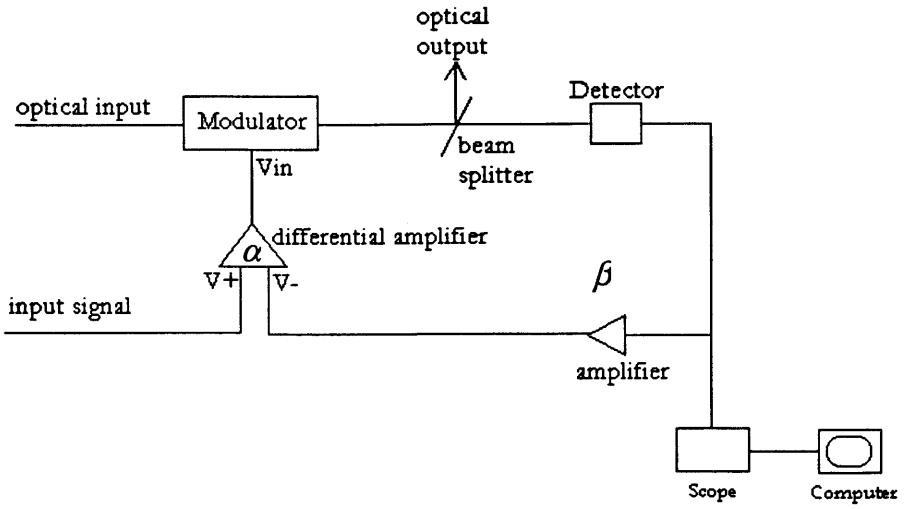


Figure 25: Closed loop modulator block diagram

## Mathematical Formulation

The response function of a general modulator is non-linear, Equations 4 & 5, Chapter 1. Since this function is non-linear, we cannot derive an explicit input-output relationship of the closed loop system. If $v_{in}$ is the differential amplifier drive, then a generalized input-output function of the modulator is

$$P_{out} = P_{in} f(\gamma(v_{in} + v_o))$$

Equation 37: Implicit input-output relationship in non-linear closed loop system.

where $\gamma = \frac{\pi}{2V_\pi}$. $v_o$ denotes a static bias voltage and $V_\pi$ is voltage needed to change the modulator phase by $\pi$.

We shall now derive the implicit input-output relationship of the feedback system. The detector produces a current proportional to the incident optical intensity. This current is then dropped across a resistor (not shown) and the resulting voltage amplified and used to drive the differential amplifier. Thus

$V_- = K\beta P$ where $K$ is a constant associated with the detector parameters and $P = P_{out}$. The differential amplifier amplifies the difference of $V_+$ and $V_-$ such that the modulator drive is given by

$$v_{in} = \alpha(V_+ - V_-) = \alpha(v - K\beta P)$$

Equation 38: Expression for input differential drive voltage.

where $v$ is the input signal. In a dynamic sense, the output optical power is then given by

$$P = f(\gamma\{\alpha[v + v_o - \beta KP]\})$$

Equation 39: Implicit transfer function of closed loop (non-linear) modulator system.

where $\gamma = \frac{\pi}{2V_\pi}$ as before. It is assumed that the static phase is added phenomenologically in the input signal, i.e., the biasing voltage is added with the signal and is part of the feedback loop. Since all we are interested in is relative amplitudes of $P$ and $v$ i.e., the size of the harmonics, Equation 39 can be inverted and then expressed as a function of the input voltage $v$ without worrying about getting an expression for $P$. Let $g$ be the inverse of $f$, $g(x) = f^{-1}(x)$ for properly defined range of $x$. Since $f$ is non-linear, so will be $g$. Equation 39 becomes

$$g(P) = \gamma(\alpha[v + v_o - \beta KP])$$

Equation 40: Inverse of Eqn 39.

or

$$v = \beta KP - v_o + \frac{g(P)}{\alpha\gamma}$$

Equation 41: Eqn 40 expressed as a function of P.

Equation 41 is very instructive. The last term, $\frac{g(P)}{\alpha\gamma}$, is the only non-linear part of the equation. It then follows that we can reduce modulator non-linearities **arbitrarily** by increasing the differential amplifier gain.

## Correcting Fabrication Uncertainties

Equation 41 also shows that the more linearized a modulator is (through, for example, the optimized design techniques discussed in Chapter 2), the less gain will be required to reduce the non-linear terms to a given level. This fact is important because the differential amplifier gain is limited by its frequency response. Given that the gain-bandwidth product of the differential amplifier is fixed, a lower gain implies higher bandwidth and hence faster device.

To see why a more linearized modulator would require less differential amplifier gain to achieve a given distortion level, we express $g(P)$ in Taylor series expansion around $P = 0$ and plug into Equation 41:

$$v = \beta KP - v_o - \frac{1}{\alpha\gamma}[m_o + m_1 P + m_2 P^2 + m_3 P^3 + m_4 P^4 + \ldots + m_n P^n]$$

Equation 42: Eqn 41 with Taylor expanded g(P).

where $m_i$'s are constants. If the modulator is properly biased, even order terms will vanish. Suppose the modulator has already been linearized using the linearization techniques in Chapters 1 & 2, then the amplitudes of higher harmonics, denoted by the size of $m_i$'s, will be small. This implies that a smaller differential gain will be required to achieve a given distortion level according to Equation 42.

Additionally, any fabrication uncertainties can also be corrected using this simple closed-loop feedback method. Fabrication uncertainties, e.g. limited resolution in masks used to fabricate coupling sections in the directional coupler, will lead to

imprecise modulator parameters. As shown in the last chapter, an error in the fifth decimal place (.005% error) of coupling-length leads to a 40dBf error. These types of errors can be corrected by appropriate choice of the differential gain, $\alpha$. The next section is an example of a theoretical design that uses electrical feedback to achieve -60dBf reduction in harmonic terms. It is shown that a relatively small differential amplifier gain is required.

## An Example of Feedback Linearization

As an example, let's take a simple interferometric-type modulator, e.g., a Mach-Zehnder. It is understood that this method works for any non-linear transfer function. We only choose a Mach-Zehnder interferometer for its algebraic ease and because of its current importance and popularity.

From Equation 4 in Chapter 1, and assuming that each guide of the Mach-Zehnder has the same propagation constant, we get the following input-output relationship:

$$f(v) = \cos^2(\tfrac{\pi}{2V_\pi}[v_{in} + v_o])$$

Equation 43: Output power for a directional coupler.

Or

$$f(v) = \frac{1}{2}[1 + \cos(\tfrac{\pi}{V_\pi}[v_{in} + v_o])]$$

Equation 44: Same as Eqn. 43, re-expressed.

Using Equation 39,

$$P = \frac{1}{2}[1 + \cos(\tfrac{\pi}{V_\pi}\alpha[v + v_o - \beta KP])]$$

Equation 45: Implicit Eqn for input-output relationship of MZI with feedback

where as before, $v_{in}$ is the modulator drive voltage from differential amplifier, $v$ is the input signal and $v_o$ is a voltage bias applied at the signal source. For quadrature biasing, $P = \frac{1}{2}$ when $v = 0$. This implies, from Equation 45, that

$$v_o = \frac{1}{2}\left[\beta K + (2m+1)\frac{V_\pi}{\alpha}\right]$$

Equation 46: Expression for bias voltage for DC with feedback.

where $m = 0,1,2,3,\ldots$ Equation 46 gives the designer the flexibility of choosing $v_o$ according to other design parameters by appropriate choice of $m$.

Inverting Equation 39, we get

$$v(P) = \beta K P - v_o + \frac{V_\pi}{\pi\alpha}\cos^{-1}(2P-1)$$

Equation 47: Eqn 45 inverted to get an explicit expression of v as a function of P.

Expanding Equation 47 around $P = \frac{1}{2}$ for quadrature biasing, we get

$$v(P) = \left(\frac{\beta K}{2} - v_o + \frac{V_\pi}{2\alpha}\right) + \left(\beta K - 2\frac{V_\pi}{\pi\alpha}\right)\left(P-\frac{1}{2}\right) - \frac{4}{3}\frac{V_\pi}{\pi\alpha}\left(P-\frac{1}{2}\right)^3 - \frac{12}{5}\frac{V_\pi}{\pi\alpha}\left(P-\frac{1}{2}\right)^5$$
$$- \frac{40}{7}\frac{V_\pi}{\pi\alpha}\left(P-\frac{1}{2}\right)^7 - \frac{140}{9}\frac{V_\pi}{\pi\alpha}\left(P-\frac{1}{2}\right)^9 - \cdots$$

Equation 48: Eqn 47 expanded around $P = \frac{1}{2}$.

Letting $t = P - \frac{1}{2}$ in Equation 48 corresponds to shifting the $v$ vs. $P$ curve by half a unit along the $P$ axis and leaves the equation unchanged in all other regards. Making this coordinate shift and substituting for $v_o$ from Equation 46 with $m = 0$ into Equation 48 leads to

$$v(t+\tfrac{1}{2}) = \left(\beta K - 2\frac{V_\pi}{\pi\alpha}\right)t - \frac{4}{3}\frac{V_\pi}{\pi\alpha}t^3 - \frac{12}{5}\frac{V_\pi}{\pi\alpha}t^5 - \frac{40}{7}\frac{V_\pi}{\pi\alpha}t^7 - \frac{140}{9}\frac{V_\pi}{\pi\alpha}t^9 - \cdots$$

Equation 49: Eqn 48 simplified, with $v_o$ substituted and a $t = P - \frac{1}{2}$ coordinate shift.

Equation 49 is also instructive. It says that by proper choice of detector parameters $\{\beta, K\}$, we can choose the bracketed term to be as close as possible to unity, and choose a high differential gain, $\alpha$, to remove the rest of the non-linear terms, resulting in a highly linearized modulator response with a $P$ vs. $v$ slope of 1. In some applications, a steeper $P$ vs. $v$ slope is desirable because this leads to lower modulation voltages for any given device. Again, Equation 49 is completely customizable to such needs.

## Distortion Levels

To get the differential amplifier gain required to gain a -60dB reduction in harmonic, we will assume that the harmonic distortion is due to the 3rd and 5th order terms in Equation 49. Following Burns[9], we get the expression for distortion as

$$20\log_{10}\left[\frac{\frac{V_\pi}{\pi\alpha}\left(\frac{4}{3}+\frac{12}{5}\right)}{\beta K - 2\frac{V_\pi}{\pi\alpha}}\right]$$

Equation 50: Expression for harmonic distortion in feedback modulator.

Note that Equation 49 is an expression of "power harmonics", i.e., harmonics are in terms of power as opposed to the more usual expression in terms of signal amplitudes [Equation 49 expresses an inverse relationship] . We maintain that since all we are interested in is the relative sizes of harmonic or non-linear terms vs. the linear portions, the two formulations are equivalent.

Equation 50 is plotted in Figure 26. As can be seen, a modest differential gain of about $\alpha = 80$ is required to achieve third and fifth distortion level of -60dB. The plot is made with $\beta K = 60$.

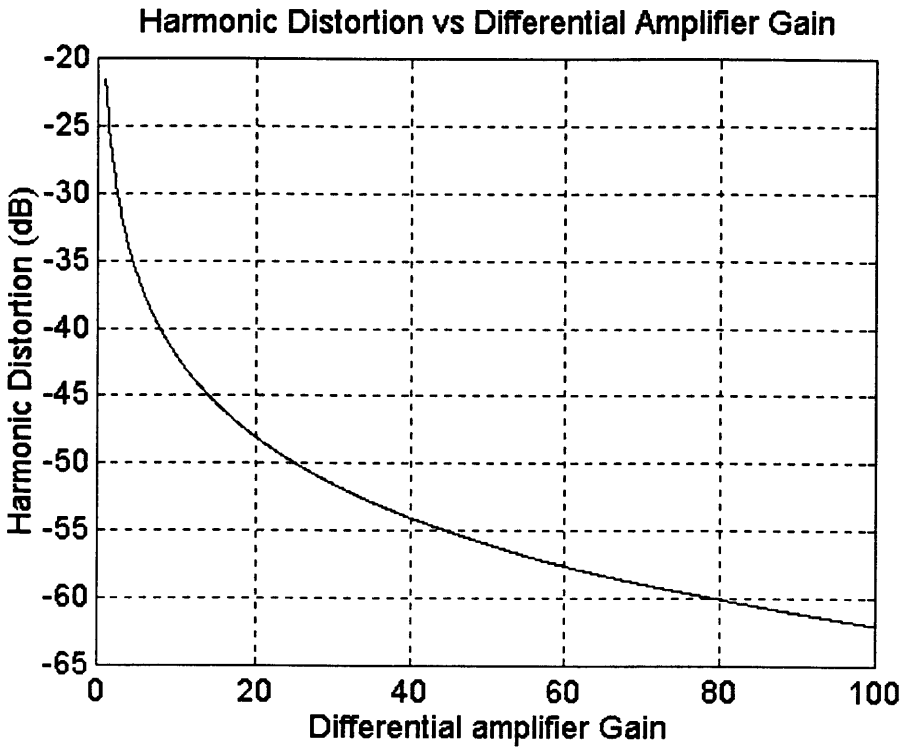


Figure 26: Plot of distortion level vs. differential amplifier gain.

## Theoretical Results

First, we note from the feedback setup of Figure 25 that the case when $\beta = 0$ and $\alpha = 1$ is equivalent to having no feedback at all. The following plots show the input-output relationship of a typical Mach Zehnder modulator with $V_\pi = 4volts$. The non-feedback case is compared with those with various gain settings.

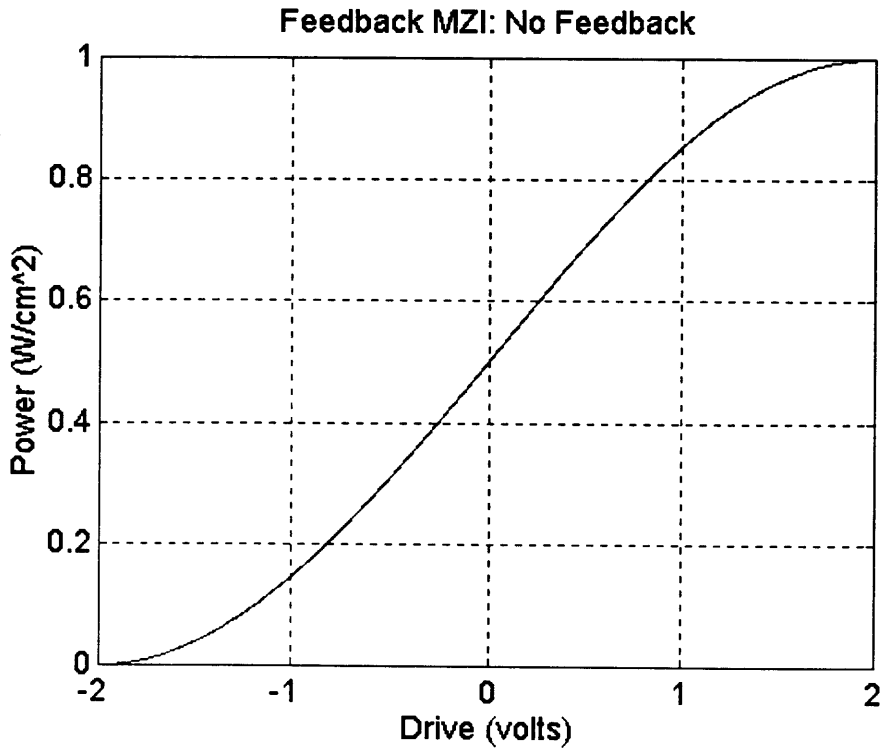


Figure 27: Directional Coupler with no Feedback, $\beta = 0,\ \alpha = 1.$

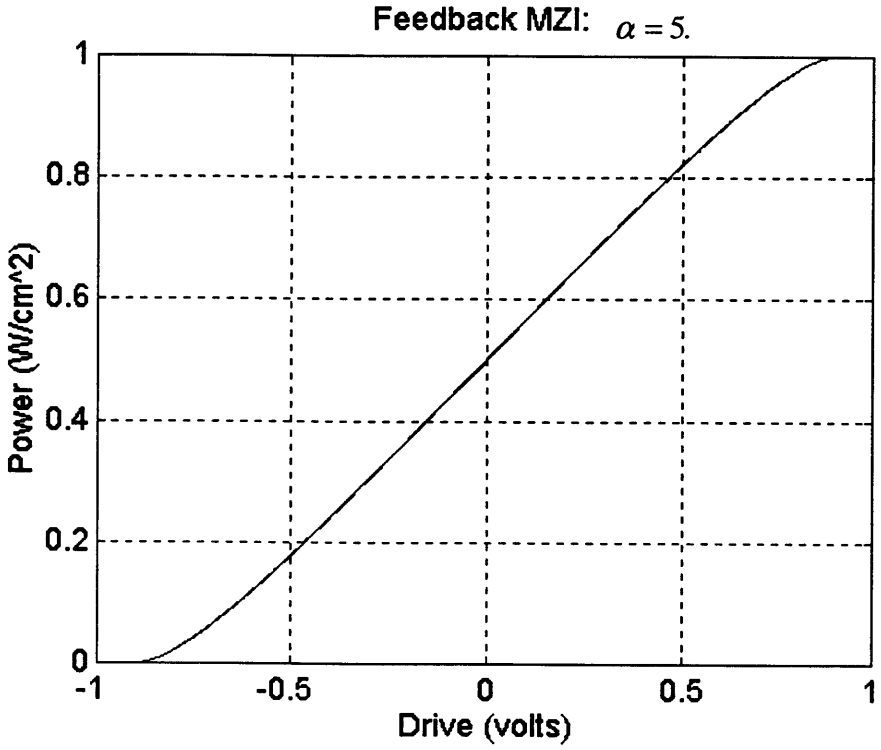


Figure 28: Directional Coupler with Feedback, $\beta = 1$, $\alpha = 5.$

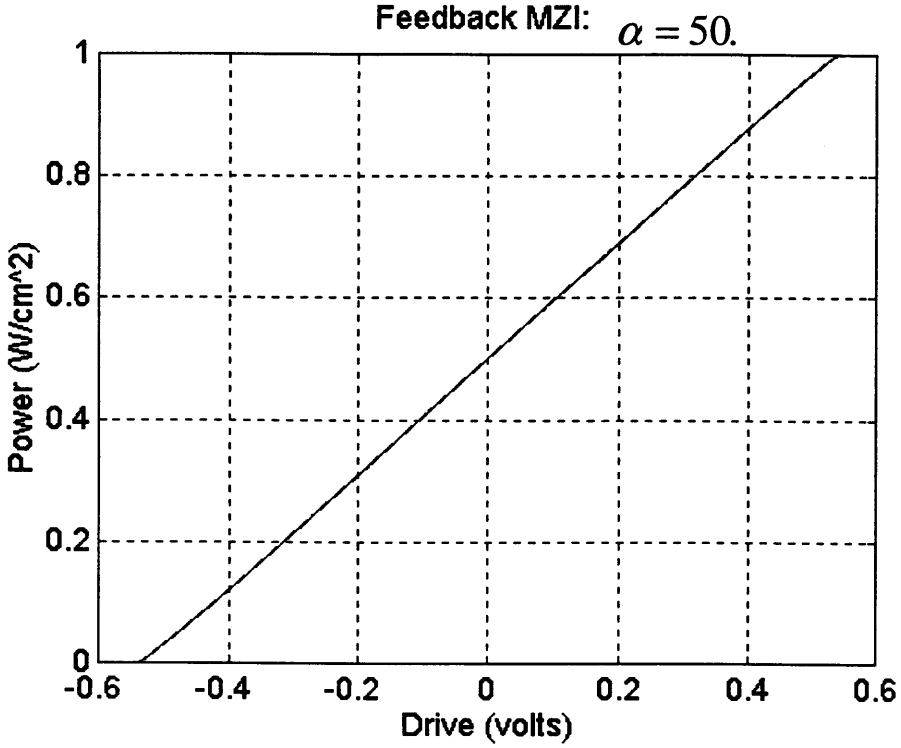


Figure 29: Directional Coupler with Feedback, $\beta = 1,\ \alpha = 50.$

As can be seen from the figures above, for $\alpha = 50$, the response of the modulator is essentially linear in this theoretical model.

## Fundamental Feedback Delay-Line Frequency Limit

The feedback setup shown in Figure 25 suffers from a fundamental ceiling modulation frequency. This is due to the fact that the feedback signal suffers propagation delays through the electrical devices and wires. Even for extremely short devices, these delays are significant given the high modulation frequencies that would be used in all-optical CATV transmission systems (tens to hundreds of Gigahertz). We will now determine what this theoretical modulation frequency ceiling is using off-the-shelf components.

With integrated laser diodes at 1.3 $\mu m$ now possible, the length of the whole system is now largely due to the length of the modulator. For lithium niobate modulators, this is about 2 inches, and using electrical propagation speed of 1 foot/ns, we get the propagation delay in the feedback loop due to wires alone is about $\frac{1}{6}$ ns. However, the electrical propagation delays can be significant across the amplifiers. Using relatively old (1993 figures on video amplifiers) off-the-shelf elements, the combined feedback propagation delay is 5 ns, giving rise to a ceiling modulation frequency in the feedback model of about 200 MHZ. We envision significantly higher modulation frequencies using current state-of-the-art components. Furthermore, with integration of the amplifiers in a single chip, the modulation frequency can further increase because of better optimization of chip parameters and proximity of all the electrical components.

*Chapter 4*

# Experimental Results and Analysis

We present here the results of feedback linearization using the ideas discussed so far. It is first shown that a transversely modulated Lithium Niobate crystal with proper input/output laser polarizations has the identical non-linearity found in any interferometric-type modulator.

## The Transverse Electro-Optic Modulator[3]

Figure 30 shows a Lithium Niobate ($LiNbO_3$) crystal driven in transverse mode whereby the electric field is applied normal to the direction of propagation. $LiNbO_3$ is a birefringent crystal which means that it supports two distinct, mutually orthogonal polarization modes each with a unique index of refraction and hence propagation constant. These are called ordinary and extra-ordinary rays with indices of refraction $n_o$ and $n_e$ respectively. The two indices of refraction are associated with two crystal directions referred to as the principal axes. Input polarizations parallel to one of the principal axes at the crystal input exits with it's polarization unchanged because it 'sees' only a single index of refraction.

When an electric field is applied as in Figure 30, the crystal principal axes are in effect rotated (primed quantities in Figure 30) in proportion to the applied field. The full analysis can be found in Yariv[3] but essentially the crystal splits the incoming field into two polarizations, each with different propagation constant. The input polarizer ensures equal electric field vectors and hence power, into the two polarization modes.

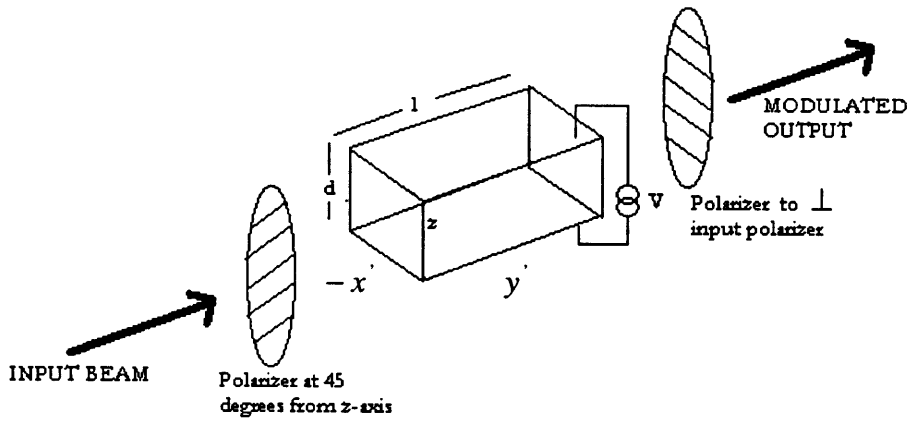


Figure 30: Transverse electro-optic amplitude modulator[3].

Inside the crystal, the two polarizations acquire a phase difference which is a function of applied voltage. It can be shown[3] that this phase difference, in the transverse modulation mode, is given by

$$\Gamma = k_o l\left[(n_o - n_e) + \frac{n_o^3}{2} r_{63}\left(\frac{V}{d}\right)\right]$$

Equation 51: Expression for phase difference between ordinary and extra-ordinary rays in Lithium Niobate crystal. After Yariv[3].

$k_o$ is free space propagation constant, $l$ is the length and $d$ the width of the crystal as shown in Figure 30. $r_{63}$ is an electro-optic coefficient in the $z$ direction as in Equation 1 from Chapter 1. Note that the crystal has a natural bias in the absence of applied voltage given by

$$\phi_o = k_o(n_o - n_e).$$

Equation 52: Natural bias for transversely modulated lithium niobate crystal.

If the amplitudes of the two waves are denoted by $A$ (their equality is ensured by the first polarizer at $45^0$ to the z-axis ), then at the output of the crystal, the two optical fields are given by

$$E_x(l) = Ae^{-j\Gamma}$$

$$E_z(l) = A$$

Equation 53: Expression of optical field at output transversely modulated $LiNbO_3$ crystal.

The output polarizer passes the components of these two fields along its axis and adds them vectorially. The result is

$$E_{out} = \frac{A}{\sqrt{2}}\left(1 + e^{-j\Gamma}\right)$$

Equation 54: Output field

The modulated output is then given by

$$I_{out} \propto E_{out}E_{out}^{*} = \frac{A^2}{2}\left[1 + \cos(\Gamma)\right]$$

Equation 55: Output power expression for transversely modulated lithium niobate crystal.

which is identical in form with the output of a Mach-Zehnder interferometer considered in Chapter 1 [Equation 4].

We have thus shown that using the modulator in Figure 30 in our feedback linearization experiments captures the essential physics of any interferometric-type electro-optic modulator.

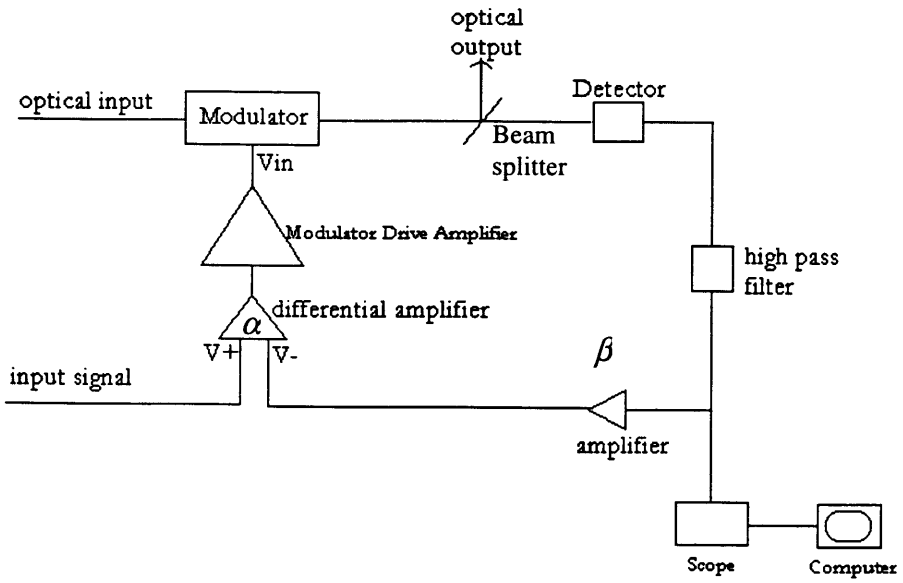


Figure 31: Experimental setup to verify feedback linearization.

# Experimental Setup

The experimental setup used is shown in the block diagram of Figure 31. The input signal is zero-bias sinusoidal AC signal. The modulated output optical signal is detected and high-pass filtered to remove the DC offset added by the detector. This allows for better tuning of the inputs to the differential amplifier as any DC offset in detected signal is amplified many times by the differential amplifier. The high pass filter was implemented using a simple R-C circuit.

# Equipment

The following equipment was used:

- Lithium Niobate crystal, $l \approx 2cm$ and $d \approx 2mm$.
- Programmable Gain Differential Amplifier, AD625 Analog Devices, Differential Gain = $\alpha$.

- Instrumentation Amplifier, AD620, Analog Devices in single-ended operation; Gain = $\beta = 1$.
- Model 5700 Krohn-Hite signal generator.
- Uniphase 20mW HeNe laser source.
- Generic photo-diode in reverse biased mode.
- Model 54502 GPIB-fitted Hewlett Packard Digitizing Scope.
- A high pass filter to block DC-offset in detector signal.
- Custom-built Drive Amplifier with high frequency roll-off ~ 100kHz.
- IBM PS/2 Personal Computer with GPIB data collection interface card.

# Experimental Considerations

## Modulation Frequency

The detector used had frequency roll-off, $f_{3dB} \approx 20kHz$. This implies that the following demonstration was essentially low-frequency. High frequency operation would be limited only by the electronics used but current state of the art using RF instrumentation amplifiers ensures that no such limitation encumbers the feedback linearization technique. The only fundamental limit to this method is the feedback delay-line limit discussed at the end of Chapter 3.

## Equipment Non-Linearity

In order to positively trace the measured non-linearities to the modulator, it is necessary to ensure that none of the other equipment is generating any non-linearities in the spectrum we expect modulator non-linearities to be. To this end, we characterized all the electronic drive equipment for non-linearities and largely found any non-linearities to be much lower than the dominant harmonic distortion term produced by the modulator. Detailed results are presented next.

Signal Generator

Ideally, we need a reference signal source with no non-linearities. In practice this is rarely true. To characterize the signal source, we simply feed the digitizing scope various amplitude sinusoids via high impedance probe. The output signal is then analyzed for its spectral content. A low frequency signal (1.8kHZ) was used. A typical output at about 400mV amplitude is shown in Figure 32. It is a normalized plot of decibels below fundamental i.e., at each sample frequency, we calculate how much lower the signal power is compared to the fundamental:

$$dB = 10 * \log_{10}\left[\frac{signal\_power(f)}{fundamental\_power}\right]$$

Equation 56: dB expression used in experiments.

As can be seen from the figure, the largest harmonics (noise) are below -80dB.

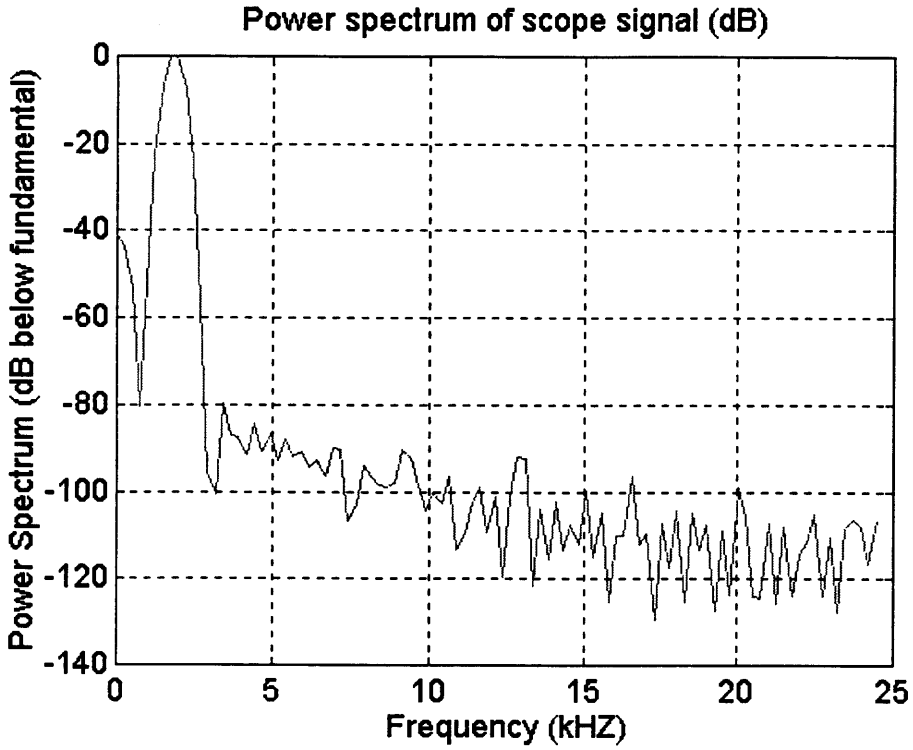


Figure 32: Power spectrum of signal generator signal.

Differential Amplifier

To characterize the differential amplifier, we drive a load with no non-linearities like a resistor and then analyze the output for harmonic content. A resistor of value $R_{load} = 2k\Omega$ was used. The differential amplifier was also found to be largely linear. Harmonics were found to be mostly below -80dB and could as well have been random noise. Two sample results are shown below: a typical case with Gain=5 and 865mV input sinusoid, and a worst case of Gain=41 and input amplitude of 300mV, Figures 33 and 34.

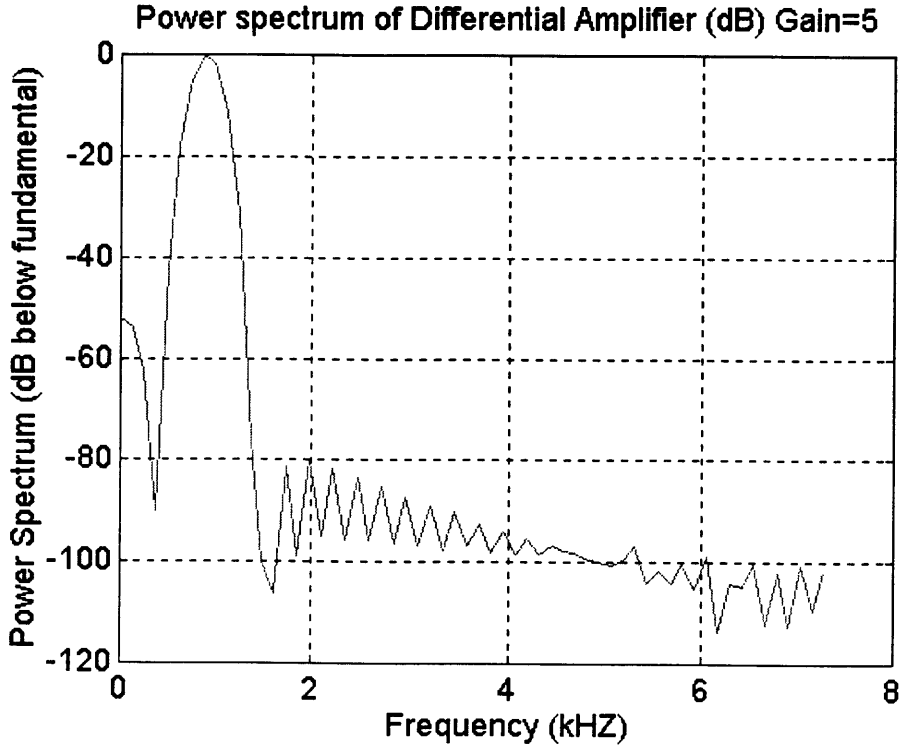


Figure 33: Differential amplifier output signal spectrum: Gain=5, input-865mV sinusoid.

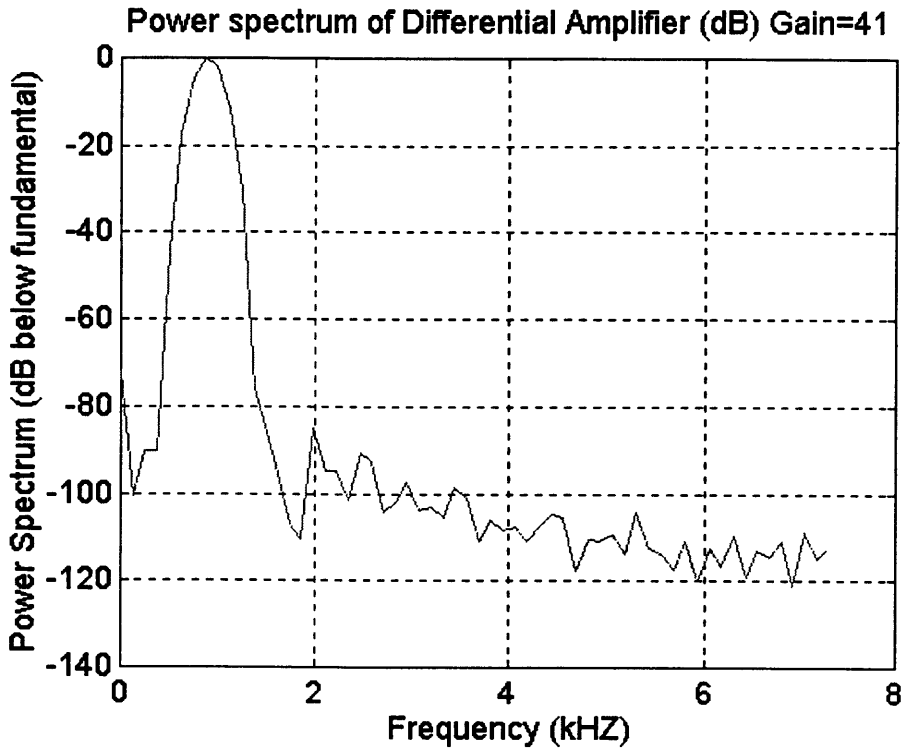


Figure 34: Differential amplifier output signal spectrum: Gain=41, input-300mV sinusoid

Drive Amplifier

The drive amplifier was found to have significantly higher harmonics. The highest harmonic was found to be around -62dB below fundamental at 700mV input to amplifier. Two typical results are shown in Figures 35 and 36. As will be shown next, these harmonic levels are way below those produced by the modulator so we can safely ignore them as a significant factor in our final result.

Detector

The detector wasn't characterized for lack of an accurate method. However because the detector is part of the feedback loop, any non-linearities in the detector can be considered lumped in the modulator non-linearity. The feedback circuit then linearizes the detector voltage. At any rate, for a linear detector, the

modulated output optical power will not contain any modulator non-linearities for sufficiently high differential amplifier gain.

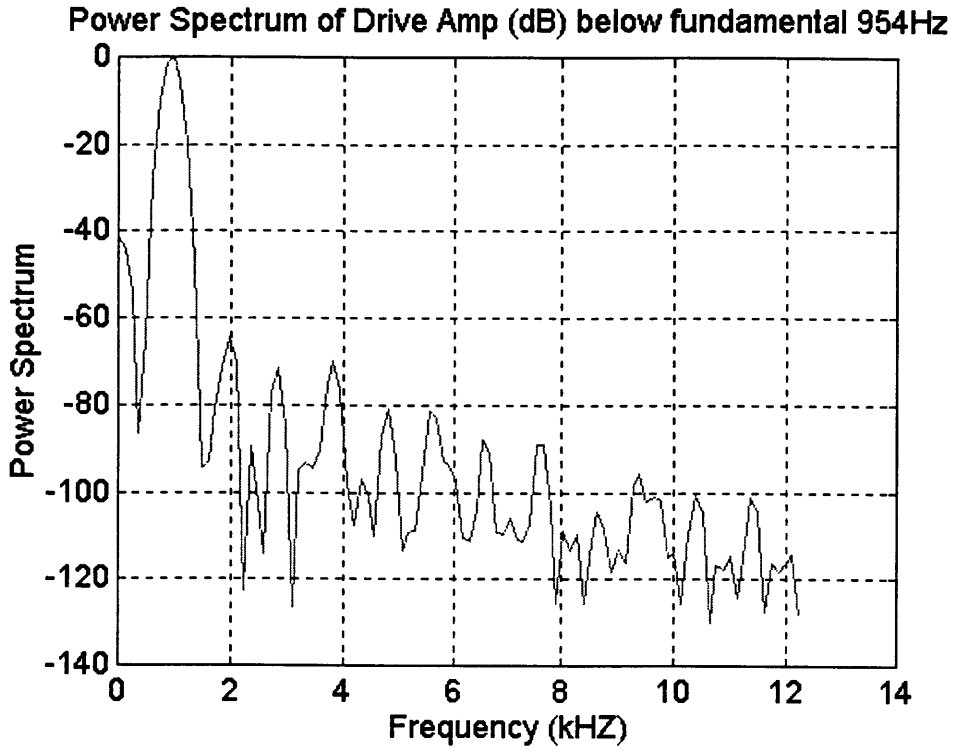


Figure 35: Modulator Drive Amplifier harmonic characteristics.

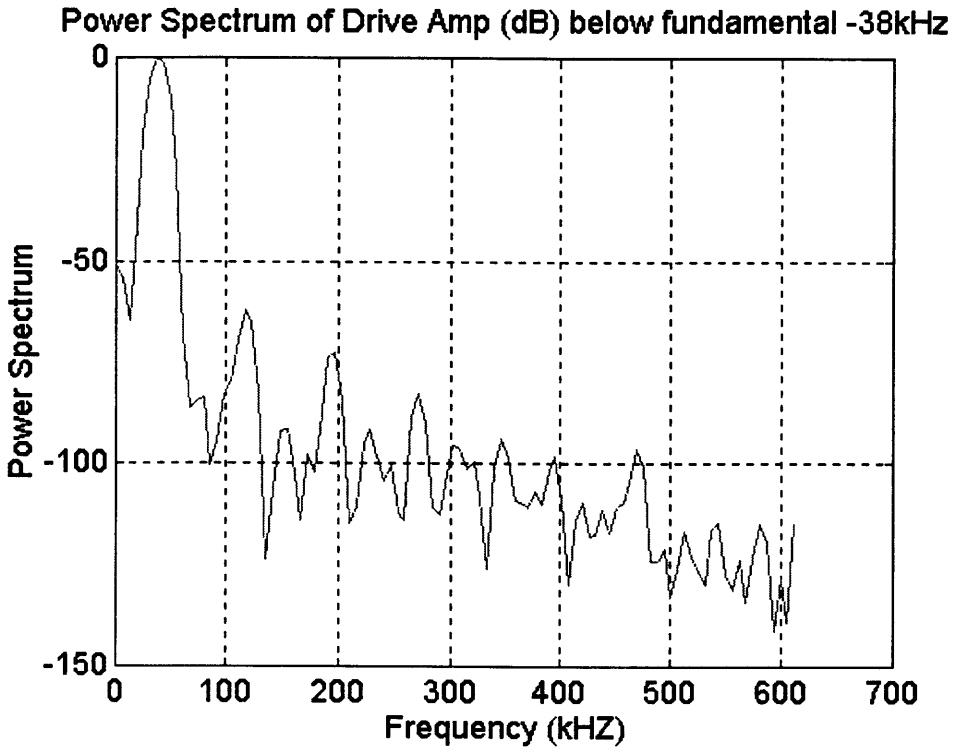


Figure 36: Modulator Drive Amplifier harmonic characteristics (high frequency).

## Linearization Results

Using the setup of Figure 31, two sets of experiments were run: one with and the other without feedback. The feedback differential amplifier gain was set at $\alpha = 41$ and the amplifier gain, $\beta$ was unity. Distortion here is defined as the size of the largest harmonic, in this case the first harmonic. In decibels, the distortion is:

$$10 * \log_{10}\left[\frac{l\arg est\_harmonic}{fundamental}\right]$$

Equation 57: Expression for definition of distortion as used in experimental data.

Three input amplitudes were used for each case and the results found to match expectations pretty closely. The distortion level increased with increasing input amplitude or modulation depth. The feedback case was also found, on average, to have about 20dB reduction in distortion. The results are plotted in Figures 37 to 42. Figure 43 then plots the distortion reduction as a function of detected output level which is a measure of modulation depth.

A plot of harmonic distortion vs. $\alpha$ is also included in Figure 44. For $\beta K = 1$, which matches the experimental setup within an order of magnitude because the detector was not fully characterized (I suspect $\beta K < 1$ in actual experiment setup), we theoretically predict a distortion reduction of about -18dB. This is close to observed value of -20dB reduction.

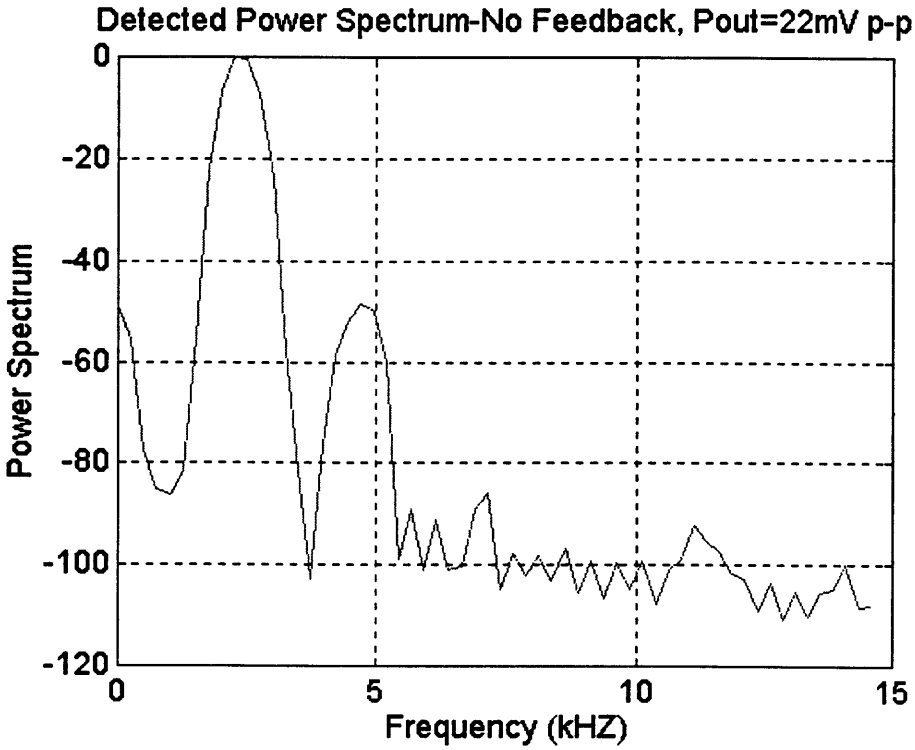


Figure 37: Distortion level for case: no feedback, output level=22mV.

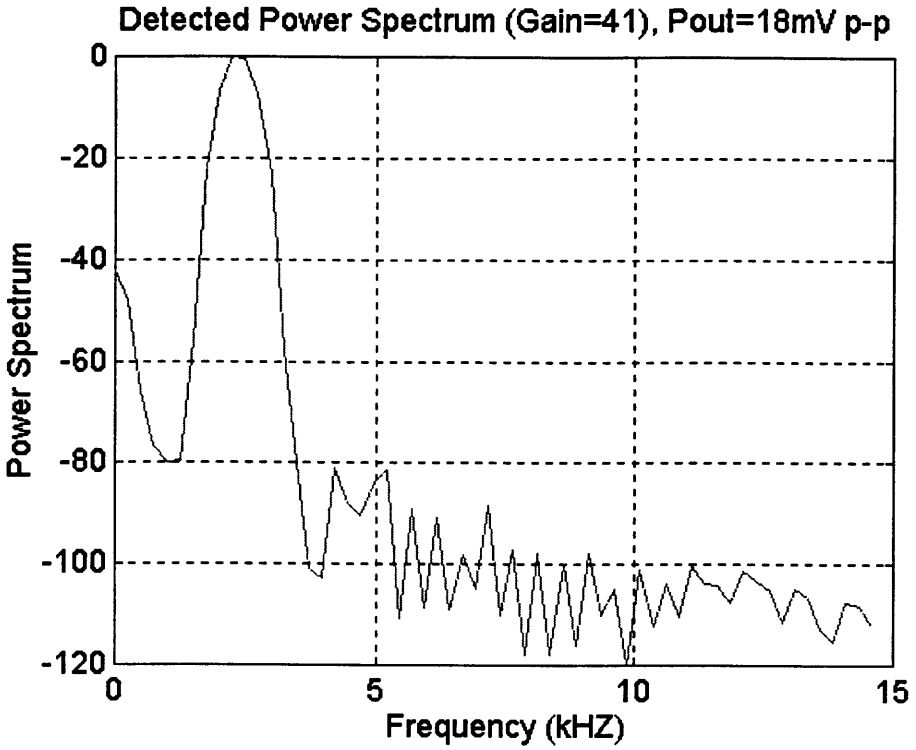


Figure 38: Distortion level for case: feedback, output level=18mV.

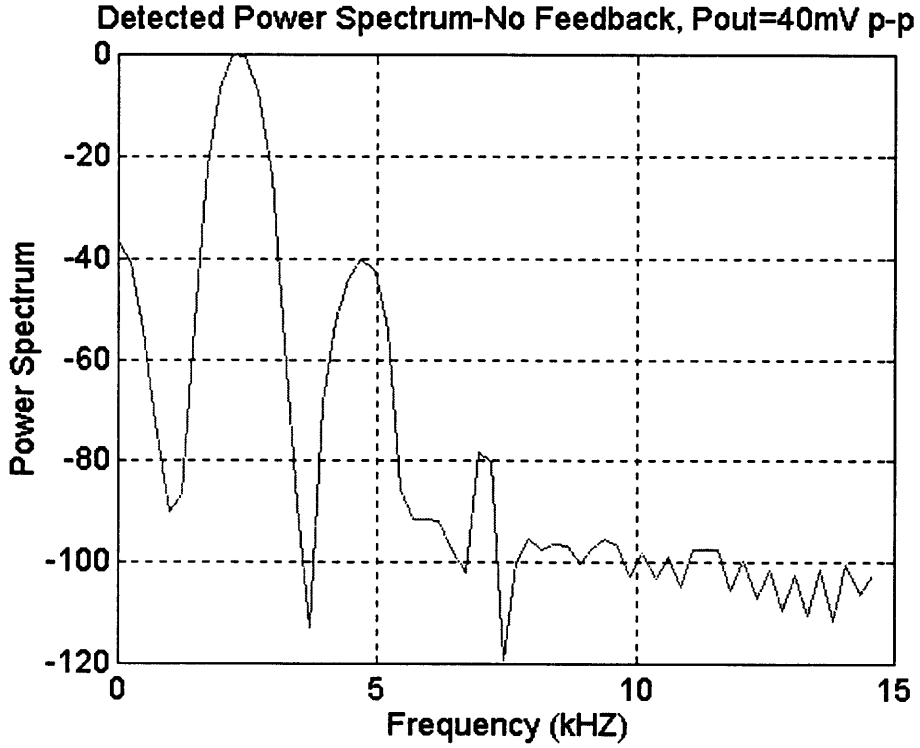


Figure 39: Distortion level for case: no feedback, output level=40mV.

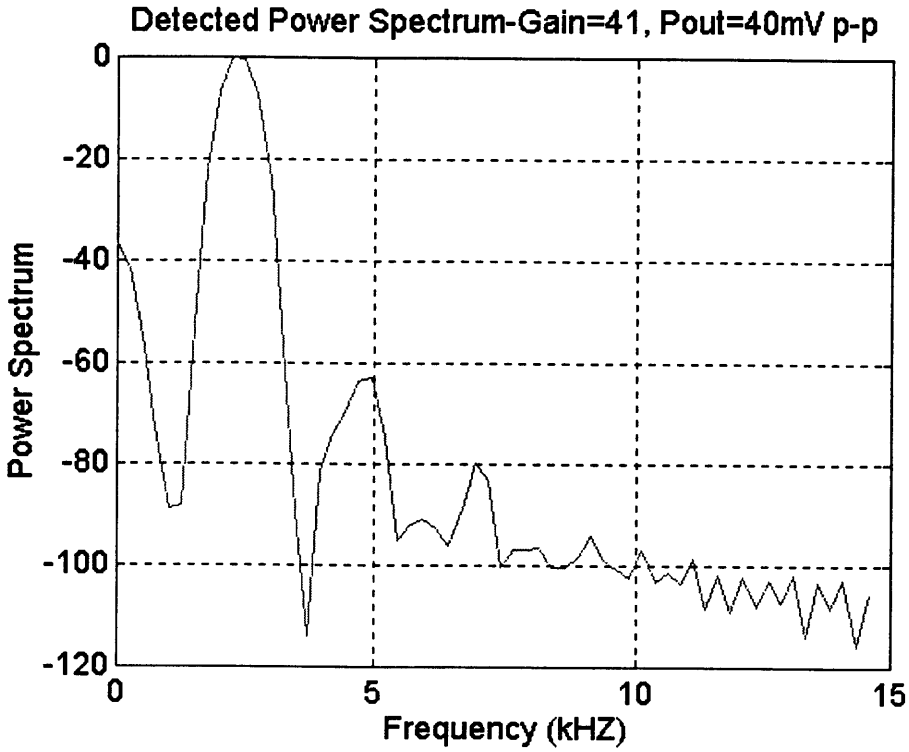


Figure 40: Distortion level for case: feedback, output level=40mV.

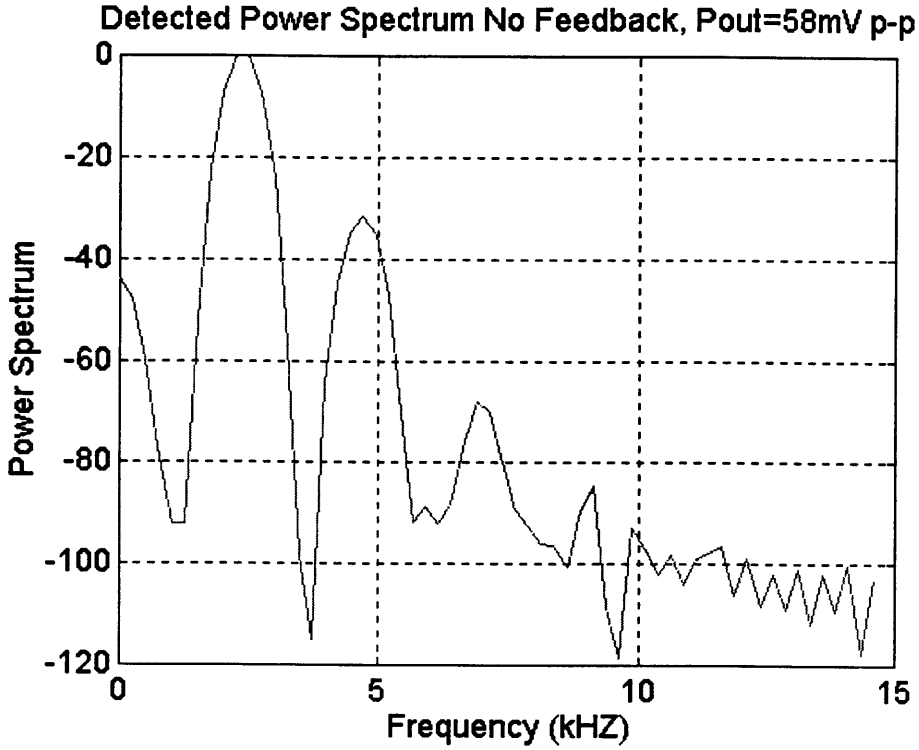


Figure 41: Distortion level for case: no feedback, output level=58mV.

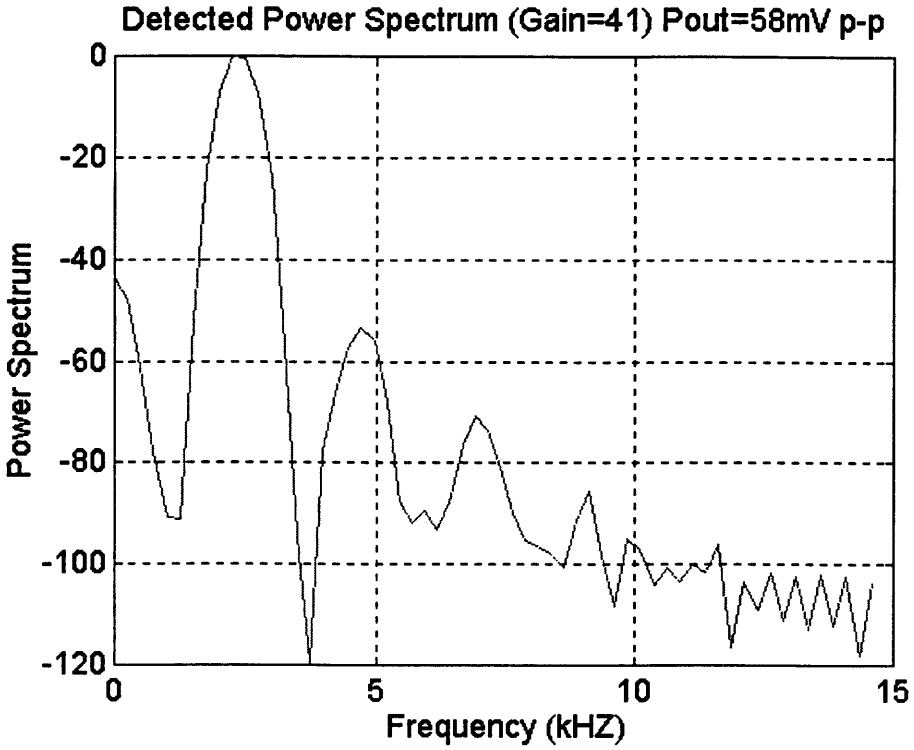


Figure 42: Distortion level for case: feedback, output level=58mV.

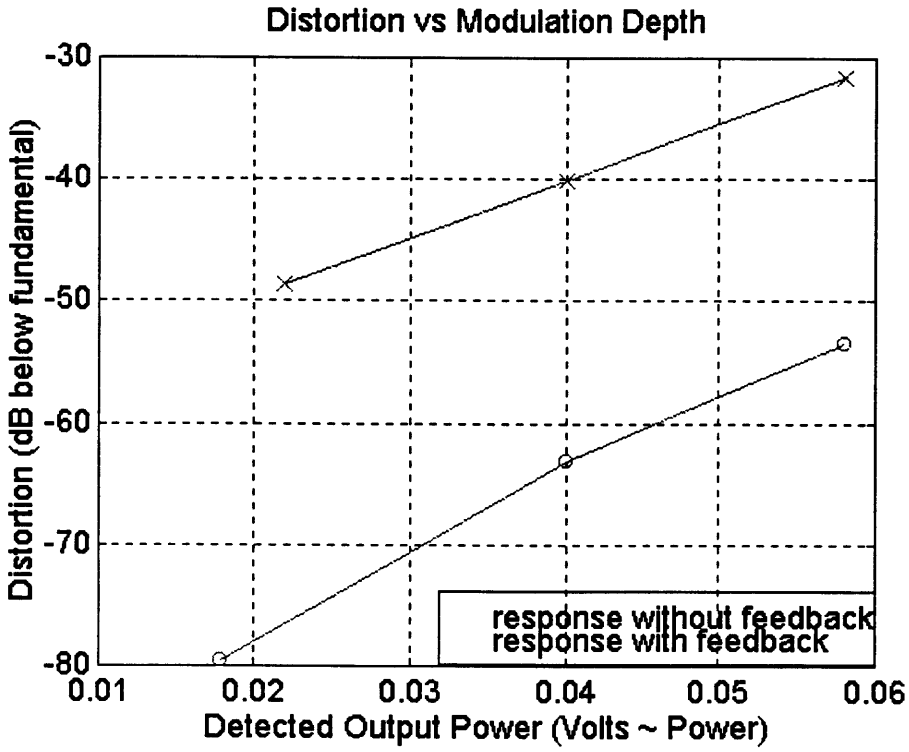


Figure 43: Plot of distortion level vs. detected output power level.

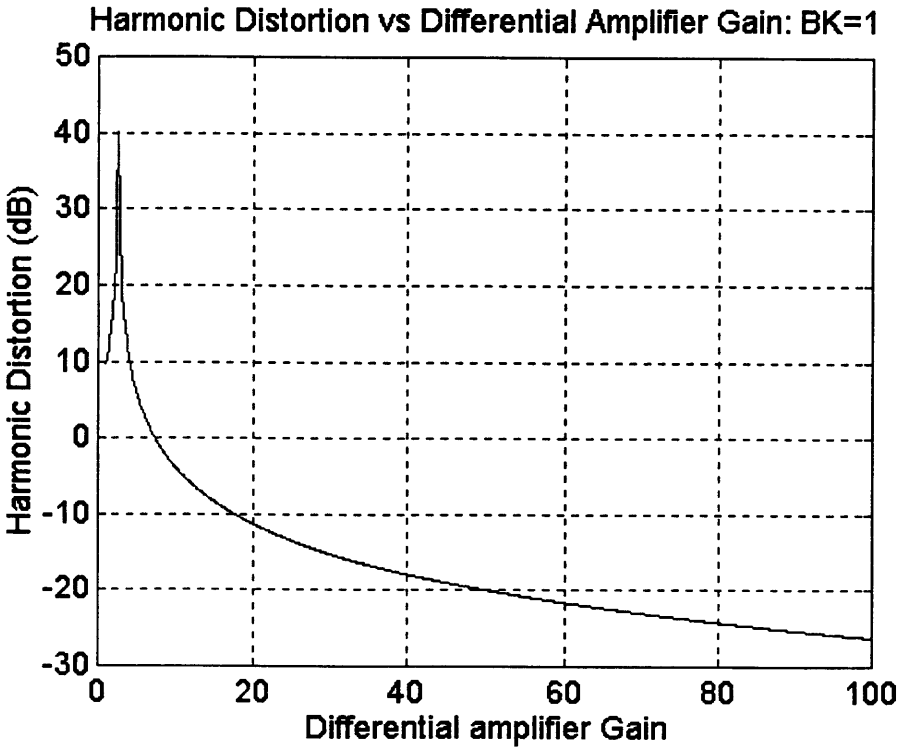


Figure 44: Plot of theoretically expected harmonic distortion vs. differential feedback gain for BK=1. This case matches experimental setup to within an order of magnitude.

## Note on Spectral Analysis

All the spectral analysis done here employed Matlab's signal processing toolbox. One major concern was equipment noise and whether this would drown some small harmonic terms, especially in the characterization experiments of the previous sections.

All the data was taken using an IBM PS/2 computer running Quick-Basic and fitted with a GPIB interface card connected to a digitizing oscilloscope. To ensure that noise was discriminated against, two approaches were taken. First, several data sets were taken per experiment, and secondly, for each successive data collection cycle, there was a randomly distributed waiting time between 1 and 5 seconds. This ensures that the oscilloscope data settles down before another data set is sampled. A set of 10 sample data sets was then taken, convolved with each other reversed, the convolutions averaged and then the Fourier transform of the average taken to get power spectral density. Since equipment noise is random while the signal isn't, the harmonics can then be seen as clear spikes in a sea of noise-floor. All the data collection routines can be found in Appendix B.

## Summary

We have demonstrated the concept of feedback linearization at low frequencies. The experimental results match predicted theoretical results and, except for fundamental limits on modulation predicted in Chapter 3, we expect the method to work well at high frequencies too just as predicted by the analysis of Chapter 3.

*Chapter 5*

# Conclusions and Summary

## Conclusions and Summary

All optical CATV transmission systems require extremely linear integrated electro-optical modulators in order to achieve strict distortion tolerances allowable for faithful transmission of video images. These integrated optical modulators devices are based on the interference of two optical fields or mode coupling, both resulting into a very non-linear transfer function. Some engineering is then required to tailor the response of these devices to be as linear as required.

Many authors have proposed several solutions[5,6,7,8,9]. Most of these solutions rely on optimizing device parameters such as coupling strength/lengths and constants, phases, and sometimes the coupling profile. Accurate solutions are often possible, but the devices can be quite complicated[10] and/or very long[9]. Furthermore, with as strict distortion levels as -60dB, any slight deviations from the prescribed solutions lead to large errors in distortion levels of operational devices. Given the uncertainties in masks dimensions during device fabrication, device parameters are bound to have errors and hence higher-than-designed for distortion levels in the actual device. Other uncertainties arise from unwanted out-diffusion[14] during titanium diffusion of Lithium niobate to form waveguides. This results in larger or otherwise undesirable waveguide shapes.

Other authors have suggested using electrical pre-distortion circuits to anticipate device distortion and correct for it from the start[13]. These have some promise but

suffer from a systemic frequency dependence in that how well the pre-distortion circuits reduces device output distortion depends on frequency.

We have a bi-focused approach that not only uses the optimization techniques prevalent in literature but combines them with a simple yet robust and effective method to reduce harmonic distortion. A feedback linearization model is presented and analyzed in detail. Using the results of the analysis, we come up with useful conclusions about how experimental parameters can be tailored to suit linearization objectives which are transparent from out formulation. Using a simple interferometric-type modulator, we demonstrate theoretical linearization by using modest gains, ensuring that frequency response considerations would not be a limitation in the feedback linearization model.

A fundamental limit on modulation frequency imposed by the feedback delay-line is derived from the feedback model. Using current state of the art laser source sizes and device propagation delays, we calculate what this limit is. We see this as the only limiting factor in using feedback linearization technique.

Experimental results based on a prototypical interferometric-type modulator are presented. The experimental results show about 20dB reduction in harmonic distortion and agree reasonably well with theoretical predictions.

# Future Work

A full realization of the feedback model needs to be undertaken. This will involve using waveguide modulators which have been linearized using device parameter optimization techniques. Based on the theoretical foundation presented in this thesis, future work would verify device operation at high modulation frequencies and do further analysis on the feedback to fully understand any instabilities from the feedback loop.

*Appendix A*

# Maple Symbolic Manipulation Program

The following Maple file was used to solve for the output power in the second guide for the 3-guide modulator discussed in Chapter 2. Maple is a symbolic manipulation package suitable for solving complicated expressions of device output power.

```
> #6/29/96
> #
> #3 waveguide device (pertubation-from-2-guide approach)
> #
> restart;
> with(linalg):
Warning: new definition for  norm
Warning: new definition for  trace

>#  First we solve for output power

>#  The following are values of k1l1=k2l2 solved in Equation 22, Chapter 2.
>
> d1 := arcsin(1/sqrt(2)):
> d2 := d1:

>#  following are expressions for k3l3 and k4l4--See Equations 28 & 29, Chapter 2
>#
> k24z := sqrt(d2^2+d4^2):
> k13z := sqrt(d1^2+d3^2):

> # vo is static phase
>assume(v0,real);
> assume(d3,real);
> assume(d4,real);
>#  m1 through m3 implement Equation 28.
>
> m1 := matrix(3,3,[1/(d2^2+d4^2)*(d4^2+d2^2*cos(k24z)), -I*d2/sqrt(d2^2+d4^2)*sin(k24z), -
d2*d4/(d2^2+d4^2)*(1-cos(k24z)),          -I*d2/sqrt(d2^2+d4^2)*sin(k24z),          cos(k24z),-
I*d4/sqrt(d2^2+d4^2)*sin(k24z),-d2*d4/(d2^2+d4^2)*(1-cos(k24z)),-
I*d4/sqrt(d2^2+d4^2)*sin(k24z),1/(d2^2+d4^2)*(d2^2+d4^2*cos(k24z))]):

> m2 := matrix(3,3,[exp(I*(2*v)),0,0,0,I,0,0,0,exp(-I*(v0-v))]):
```

```
> m3 := matrix(3,3,[1/(d1^2+d3^2)*(d3^2+d1^2*cos(k13z)), -I*d1/sqrt(d1^2+d3^2)*sin(k13z), -
d1*d3/(d1^2+d3^2)*(1-cos(k13z)),          -I*d1/sqrt(d1^2+d3^2)*sin(k13z),          cos(k13z),-
I*d3/sqrt(d1^2+d3^2)*sin(k13z),-d1*d3/(d1^2+d3^2)*(1-cos(k13z)),-
I*d3/sqrt(d1^2+d3^2)*sin(k13z),1/(d1^2+d3^2)*(d1^2+d3^2*cos(k13z))]):

># m=m1*m2*m3, Equation 28.
>
> m := evalm(&*(m1,m2,m3)):

># the following lines express output power of 2nd guide in power series
># then optimizes for the unknowns by setting higher order terms to zero.
>
> p2 := simplify(evalc(abs(m[2,2]))^2):
>
> p2out := series(p2,v,10):
>
> eqn0 := coeff(p2out,v,0):
> eqn1 := coeff(p2out,v,1):
> eqn2 := coeff(p2out,v,2):
> eqn3 := coeff(p2out,v,3):
> eqn4 := coeff(p2out,v,4):
> eqn5 := coeff(p2out,v,5):
> eqn6 := coeff(p2out,v,6):
> eqn7 := coeff(p2out,v,7):
>
> # device solutions
>
> fsolve({eqn0=1/2,eqn3=0,eqn2=0},{d3,d4,v0},{d3=.01..Pi,d4=0.01..Pi,v0=-Pi..Pi});

        {v0~ = -1.153879772, d4~ = 1.988625661, d3~ = 1.495251000}
># output power expression with solutions above.
>
> power:=evalf(subs(d4=1.495251000, d3=1.988625661, v0=-1.153879772,p2));

    power := .4999999998 - .1972936469 sin(2. v) sin( - 1.153879772 - 1. v)
        + .1972936469 cos(2. v) cos( - 1.153879772 - 1. v)
        + .08737726311 sin( - 1.153879772 - 1. v) - .01812637914 sin(2. v)
>

> # We then evaluate the higher order terms to make sure the optimization has worked.

> m0 := evalf(subs(d4=1.495251000, d3=1.988625661, v0=-1.153879772,eqn0));
                        m0 := .4999999996

> m1 := evalf(subs(d4=1.495251000, d3=1.988625661, v0=-1.153879772,eqn1));
                        m1 := .1087582743

> m2 := evalf(subs(d4=1.495251000, d3=1.988625661, v0=-1.153879772,eqn2));
                                        -9
                    m2 := .1245796489*10
```

```
> m3 := evalf(subs(d4=1.495251000, d3=1.988625661, v0=-1.153879772,eqn3));
                                        -10
                    m3 := .5990846306*10

> m4 := evalf(subs(d4=1.495251000, d3=1.988625661, v0=-1.153879772,eqn4));
                                        -11
                   m4 := -.8986269459*10
> m5 := evalf(subs(d4=1.495251000, d3=1.988625661, v0=-1.153879772,eqn5));
                    m5 := -.003625275830

> m6 := evalf(subs(d4=1.495251000, d3=1.988625661, v0=-1.153879772,eqn6));
                                        -12
                    m6 := .3594507784*10
```

# Matlab Optimization Files

We could also take the output power expression from the Maple files and use Matlab's optimization routines to minimize higher order terms. Matlab's optimization provides perhaps a better control on variable parameters. The files are included here for completeness. Refer to Matlab's optimization toolbox on how the optimization is actually set up and the options used.

```
%%%%%%%%%%%%%%%%%%%%
% Optimization Function call    %
%%%%%%%%%%%%%%%%%%%%

format long
 x =[1.5 2  2];
options(13) = 3;
options(1) = 1;
options(4) = 1e-7;
options(14) = 5e3;
options(3) = 1e-7;
options(2) = 1e-7;
vlb = [0 0 -pi];
vub = [pi pi pi];
x = constr('popt7',x,options,vlb,vub)
[f,g] = popt7(x)

%%%%%%%%%%%%%%%%%%%%%%%%
% Optimization Function definition %
%%%%%%%%%%%%%%%%%%%%%%%%

function [f,g] = popt7(x)

% x(1)=d3, x(2)=d4, x(3)=v0.

% the linear term
f =  ((-32*pi^2*x(2)*cos(x(3))*x(1)*(cos(.25*sqrt(pi^2+16*x(2)^2)))^2  +...
32*cos(.25*sqrt(pi^2+16*x(2)^2))*cos(.25*sqrt(pi^2+16*x(1)^2))*sqrt(pi^2 ...
+ 16*x(2)^2)*sqrt(pi^2 +...
16*x(1)^2)*x(2)*sin(.25*sqrt(pi^2+16*x(2)^2))*sin(x(3))*x(1)*sin(.25*sqrt(pi^2+16*x(1)^2))        +
32*pi^2*x(2)*cos(x(3))*x(1) -...
32*pi^2*x(2)*cos(x(3))*x(1)*(cos(.25*sqrt(pi^2+16*x(1)^2)))^2 +...
4*pi^2*sin(.25*sqrt(pi^2+16*x(2)^2))*sin(.25*sqrt(pi^2+16*x(1)^2))*cos(.25*sqrt(pi^2+16*x(2)^2)
)*cos(.25*sqrt(pi^2+16*x(1)^2))*sqrt(pi^2 ...
```

```
+ 16*x(2)^2)*sqrt(pi^2+ 16*x(1)^2) +...
32*pi^2*x(2)*cos(x(3))*x(1)*(cos(.25*sqrt(pi^2+16*x(2)^2)))^2*(cos(.25*sqrt(pi^2+16*x(1)^2)))^2)
/(pi^4 ...
+ 16*pi^2*x(1)^2 + 16*x(2)^2*pi^2  + 256*x(2)^2*x(1)^2)-.1);

%the second order term
g(1) = (16*pi^2*x(2)*sin(x(3))*x(1)*(cos(.25*sqrt(pi^2+16*x(2)^2)))^2 ...
+ 16*pi^2*x(2)*sin(x(3))*x(1)*(cos(.25*sqrt(pi^2+16*x(1)^2) ))^2 -...
16*pi^2*x(2)*sin(x(3))*x(1) -...
16*pi^2*x(2)*sin(x(3))*x(1)*(cos(.25*sqrt(pi^2+16*x(2)^2)))^2*(cos(.25*sqrt(pi^2+16*x(1)^2)))^2 -
...
16*cos(.25*sqrt(pi^2+16*x(2)^2))*cos(.25*sqrt(pi^2+16*x(1)^2))*sqrt(pi^2+16*x(2)^2)*sqrt(pi^2
+16*x(1)^3)*x(2)*sin(.25*sqrt(pi^2+16*x(2)^2) ...
)*cos(x(3))*x(1)*sin(.25*sqrt(pi^2+16*x(1)^2)))/(pi^4+16*pi^2*x(1)^2 +...
16*x(2)^2*pi^2 + 256*x(2)^2*x(1)^2);

%the third order term
 g(2) = (- 16/3*pi^2*x(2)*cos(x(3))*x(1) +...
16/3*pi^2*x(2)*cos(x(3))*x(1)*(cos(.25*sqrt(pi^2+16*x(2)^2)))^2 -...
8/3*pi^2*sin(.25*sqrt(pi^2+16*x(2)^2))*sin(.25*sqrt(pi^2+16*x(1)^2))*cos(.25*sqrt(pi^2+16*x(2)
^2))*cos(.25*sqrt(pi^2+16*x(1)^2))*sqrt(pi^2+16*x(2)^2)*sqrt(pi^2+16*x(1)^2) ...
-
16/3*pi^2*x(2)*cos(x(3))*x(1)*(cos(.25*sqrt(pi^2+16*x(2)^2)))^2*(cos(.25*sqrt(pi^2+16*x(1)^2)))
^2 ...
+ 16/3*pi^2*x(2)*cos(x(3))*x(1)*(cos(.25*sqrt(pi^2+16*x(1)^2)))^2  -...
16/3*cos(.25*sqrt(pi^2+16*x(2)^2))*cos(.25*sqrt(pi^2+16*x(1)^2))*sqrt(pi^2+16*x(2)^2)*sqrt(pi^
2+16*x(1)^2)*x(2)*sin(.25*sqrt(pi^2+16*x(2)^2))*sin(x(3))*x(1)*sin(.25*sqrt(pi^2+16*x(1)^2)))/(pi
^4+16*pi^2*x(1)^2 ...
+ 16*x(2)^2*pi^2+256*x(2)^2*x(1)^2);

%dc term
 g(3) = (512*(cos(.25*sqrt(pi^2+16*x(2)^2)))^2*(cos(.25*sqrt(pi^2 +...
16*x(1)^2)))^2*x(2)^2*x(1)^2+ pi^4  +...
2*(cos(.25*sqrt(pi^2+16*x(2)^2)))^2*(cos(.25*sqrt(pi^2+16*x(1)^2)))^2*pi^4 ...
- 256*x(2)^2*x(1)^2*(cos(.25*sqrt(pi^2+16*x(2)^2)))^2  -...
256*x(2)^2*x(1)^2*(cos(.25*sqrt(pi^2+16*x(1)^2)))^2 + 32*pi^2*x(2)*...
sin(x(3))*x(1)*(cos(.25*sqrt(pi^2+16*x(2)^2)))^2*(cos(.25*sqrt(pi^2 +...
16*x(1)^2)))^2 + 32*cos(.25*sqrt(pi^2+16*x(2)^2))*cos(.25*sqrt(pi^2 +...
16*x(1)^2))*sqrt(pi^2 + 16*x(2)^2)*sqrt(pi^2+16*x(1)^2)*x(2) *...
sin(.25*sqrt(pi^2+16*x(2)^2))*cos(x(3))*x(1)*sin(.25*sqrt(pi^2+16*x(1)^2)) ...
+ 16*(cos(.25*sqrt(pi^2+16*x(2)^2)))^2*(cos(.25*sqrt(pi^2 +...
16*x(1)^2)))^2*pi^2*x(1)^2  - pi^4*(cos(.25*sqrt(pi^2+16*x(1)^2)))^2  -...
pi^4*(cos(.25*sqrt(pi^2+16*x(2)^2)))^2 + 32*pi^2*x(2)*sin(x(3))*x(1) -...
32*pi^2*x(2)*sin(x(3))*x(1)*(cos(.25*sqrt(pi^2+16*x(1)^2)))^2 +...
16*(cos(.25*sqrt(pi^2+16*x(2)^2)))^2*(cos(.25*sqrt(pi^2+16*x(1)^2)))^2 *...
x(2)^2*pi^2 - 32*pi^2*x(2)*sin(x(3))*x(1)*(cos(.25*sqrt(pi^2+16*x(2)^2)))^2 +...
256*x(2)^2*x(1)^2)/(pi^4 + 16*pi^2*x(1)^2 + 16*x(2)^2*pi^2 +...
256*x(2)^2*x(1)^2) -.5;
```

*Appendix B*

# GPIB QuickBasic Program

The following file are used for data collection from oscilloscope for analysis in Matlab. It basically initializes the Hewlett Packard digitizing scope and its GPIB data collection board and transfers data between the scope and the computer. In a DOS environment the QuickBasic program is combined with other libraries that come with the GPIB interface software and linked to produce an executable. The program is self explanatory and implements the data collection strategy discussed at the end of Chapter 4.

```
' Programs collects digitized waveform from HP54502A Scope
' Written by Peter Orondo 11/96.
'
' Header information is for GPIB declarations (see GPIB
' Reference Section 4)
'
REM $INCLUDE: 'qbdecl4.bas'
'
' Declarations
DECLARE SUB FINDERR ()
DECLARE SUB GPIBERROR ()

'COMMON SHARED IBSTA%, IBERR%, IBCNT%

' Preamble opens GPIB Device
' Each command is followed by check for any errors
' open device and store identifier in variable DEV
BDNAME$ = "DEV1"
CALL IBFIND(BDNAME$, HP%)

' Check for error
IF DEV% < 0 THEN CALL FINDERR

' Here I take many different sample data so I can use fourier techniques to
' get rid of noise
DEFINT J
FOR J = 1 TO 10
```

```
CALL IBCLR(HP%)

' Error checker IBSTA is status global variable
IF IBSTA% < 0 THEN CALL GPIBERROR

'Initialize scope
EOISTRING$ = ":EOI ON"
CALL IBWRT(HP%, EOISTRING$)
IF IBSTA% < 0 THEN CALL GPIBERROR

'turn on headers
HEADER$ = ":SYSTEM:HEADER OFF;LONGFORM OFF"
CALL IBWRT(HP%, HEADER$)
IF IBSTA% < 0 THEN CALL GPIBERROR

PROBE$ = ":BNC PROBE"
CALL IBWRT(HP%, PROBE$)
IF IBSTA% < 0 THEN CALL GPIBERROR

'To get a larger-window waveform, set timebase manually
'AUTOSCALE$ = ":AUTOSCALE"
'TRANGE$ = ":TIMEBASE:RANGE 5000e-6"
'VRANGE$ = ":CHANNEL1:RANGE 20e-3"
'VOFFSET$ = ":CHANNEL1:OFFSET 0"

'CALL IBWRT(HP%, AUTOSCALE$)
'IF IBSTA% < 0 THEN CALL GPIBERROR

'CALL IBWRT(HP%, TRANGE$)
'IF IBSTA% < 0 THEN CALL GPIBERROR

'CALL IBWRT(HP%, VRANGE$)
'IF IBSTA% < 0 THEN CALL GPIBERROR

'CALL IBWRT(HP%, VOFFSET$)
'IF IBSTA% < 0 THEN CALL GPIBERROR

TIMEBASE$ = ":TIMEBASE:SAMPLE REALTIME"
CALL IBWRT(HP%, TIMEBASE$)
IF IBSTA% < 0 THEN CALL GPIBERROR

COUPLING$ = ":CHANNEL1:COUPLING AC"
CALL IBWRT(HP%, COUPLING$)
IF IBSTA% < 0 THEN CALL GPIBERROR

'Now digitize the waveform and get it into a file
SOURCE$ = ":WAVEFORM:SOURCE CHANNEL1"
CALL IBWRT(HP%, SOURCE$)
IF IBSTA% < 0 THEN CALL GPIBERROR

' Acquisition TYPE average
```

```
ACQUIRETYPE$ = ":ACQUIRE:TYPE AVERAGE"
CALL IBWRT(HP%, ACQUIRETYPE$)
IF IBSTA% < 0 THEN CALL GPIBERROR

COUNT$ = ":ACQUIRE:COUNT 4"
CALL IBWRT(HP%, COUNT$)
IF IBSTA% < 0 THEN CALL GPIBERROR

' 100 % completion criteria for each acquisition, Set format to ascii
CRITERIA$ = ":ACQUIRE:COMPLETE 100"
WFORMAT$ = ":WAVEFORM:FORMAT ASCII"
CALL IBWRT(HP%, WFORMAT$)
IF IBSTA% < 0 THEN CALL GPIBERROR

CALL IBWRT(HP%, CRITERIA$)
IF IBSTA% < 0 THEN CALL GPIBERROR

'Set the waveform full record command in order to enable us to collect 2000 points
FULLRECORD$ = ":WAVEFORM:RECORD FULL"

CALL IBWRT(HP%, FULLRECORD$)
IF IBSTA% < 0 THEN CALL GPIBERROR

'2000 (1024 in repetitive mode) points for each acqusition record
POINTS$ = ":ACQUIRE:POINTS 2000"
CALL IBWRT(HP%, POINTS$)
IF IBSTA% < 0 THEN CALL GPIBERROR

' Digitize channel
DIGITIZE$ = ":DIGITIZE CHANNEL1"
CALL IBWRT(HP%, DIGITIZE$)
IF IBSTA% < 0 THEN CALL GPIBERROR

'query for the preamble information
PREAMBLEQUERY$ = ":WAVEFORM:PREAMBLE?"
CALL IBWRT(HP%, PREAMBLEQUERY$)
IF IBSTA% < 0 THEN CALL GPIBERROR

PREAMBLE$ = SPACE$(1000)
CALL IBRD(HP%, PREAMBLE$)

'Write preamble info to a file
OPEN "PREAM" FOR APPEND AS #2
PRINT #2, PREAMBLE$
CLOSE #2
'Query the scope for the data

DATAQUERY$ = ":WAVEFORM:DATA?"
CALL IBWRT(HP%, DATAQUERY$)
IF IBSTA% < 0 THEN CALL GPIBERROR
```

```
' Read upto all the data
WAVDAT$ = SPACE$(16304)
CALL IBRD(HP%, WAVDAT$)
IF IBSTA% < 0 THEN CALL GPIBERROR

' Get output to a file
DEFINT I
OPEN "WAVDAT" FOR APPEND AS #1
'PRINT #1, WAVDAT$;

LENSTR = LEN(WAVDAT$)

FOR I = 1 TO LENSTR
VAL$ = MID$(WAVDAT$, I, 1)
IF VAL$ = CHR$(44) THEN
PRINT #1, CHR$(13)
ELSE
PRINT #1, VAL$;
END IF
NEXT I

CLOSE #1

'Return Scope to local state.
LSTATE$ = ":SYSTEM:KEY 39;KEY 36"
'RSTATE$= ":SYSTEM:KEY 36"
CALL IBWRT(HP%,LSTATE$)
'SLEEP 5
'CALL IBWRT(HP%,RSTATE$)

' Wait a little for noise to be truly random
' (We wait a random number of seconds between 1-5)

COUNT = 5*RND(1)
SLEEP COUNT
NEXT J              'main loop
END

DEFSNG I-J
SUB FINDERR STATIC
PRINT "IBFIND ERROR"
END SUB

SUB GPIBERROR
PRINT "SOME GPIB ERROR HAS OCCURED"
END SUB

 SUB PRINTOFILE
OPEN "WAVDAT" FOR OUTPUT AS #1

END SUB
```

# Matlab Spectral Analysis Program.

The following is sample matlab spectral analysis program used to get the harmonic content of sampled signals.

```
% 12/96
%This file is used to analyse noise data due to the sampling scope/signal generator. Basically, I
%take many (10) samples from the same data and then I convolve each sample with itself
%reversed and average the convolutions. I then take the fft to get power spectrum. The noise %is
somewhat 'averaged out'.

% Get the raw data from scope—collected by QuickBasic program of previous Appendix
% (un-interpreted)
datd1si;

% First of all, remove some seemingly extraneous data. These have values
% below 10
% Exit if the final data doesn't have desired number of elements.

badvalues = find(dat<10);

%  Remove these values from array
for I=1:size(badvalues,1)
dat(badvalues(I)) = [];
end

if size(dat,1) ~= 20000
error('something wrong---incorrect number of elements');
end

% Now form the signals data points from preamble matrix. Form a matrix
% with each column representing a sample of digitized waveform.
for I=1:1:10
rawmatrix(I,:) = dat((2000*I-1999):2000*I)';
end

% Now get the actual signals from mapping specified by scope,. specifying in preamble
% information from scope.
pre = [0,2,2000,1,+1.00000E-06,-1.00000E-03,0,+2.45098E-05,-1.25000E-02,16384];

xincr  = pre(5);
xorigin = pre(6);
xref   = pre(7);
yincr  = pre(8);
yorigin = pre(9);
yref   = pre(10);
```

```
[m,n]   = size(dat);

for I=1:10
 for J=1:2000
sigmatrix(I,J) = ((rawmatrix(I,J) - yref)*yincr) + yorigin;
time(J) = ((J - xref)*xincr) + xorigin;
 end
end

% Multiply data by a hamming window
for I=1:10
winmatrix(I,:) = sigmatrix(I,:).*hamming(2000)';
end

% Try convolution approach. Here, convolve each windowed signal with itself and average.
% for I=1:10
temp=winmatrix(I,:);
revmatrix(I,:)=temp(2000:-1:1);
convmatrix(I,:) = conv(winmatrix(I,:),revmatrix(I,:));
end

% Do the average of the convolutions then take the fft to get the spectrum

avematrix = zeros(1,size(convmatrix(1,:),2));
for I=1:10
avematrix = avematrix + convmatrix(I,:);
end
avematrix = avematrix./10;

% Get power spectrum

Y = fft(avematrix,4048);
Pyy = Y.*conj(Y)/2047;
f = 1/(xincr)*(0:2047)/4048;

% Plot spectrum as dB below fundamental (which I take to be the largest
% (most manifest signal)

plot(f(1:100)/1000,10*log10(Pyy(1:100)./max(Pyy(1:100))))
xlabel('Frequency (kHZ)')
ylabel('Power Spectrum (dB below fundamental)')
title('Power spectrum of scope signal (dB)')
grid
```

# References


[1] R. B. Childs and V. O'Byrne. Multichannel AM video transmission using a high power Nd:YAG laser and linearized external Modulator. *IEEE Journal on Selected Areas in Communications,* vol 8 no 7, pp1389+, September, 1990.

[2] G. E. Betts, L. M. Johnson and H. V. Roussell. Integrated-optical modulators for bandpass analog links. In, Paul Sierak, Ed, *SPIE Proceedings*, no 1371, pp 2-7, San Jose, September, 1990. SPIE.

[3] Amnon Yariv. *Optical Electronics*, Third Edition, Chapter 9. Holt, Rinehart and Winston, New York, 1985.

[4] C.H Cox III, G. E. Betts, and L. M. Johnson. An Analytical and Experimental Comparison of Direct and External Modulation. *IEEE Transactions on Microwave Theory and Technology.*, vol. 38, pp. 501-509, May 1990.

[5] B. J. Li, P. L. Liu and Y. S. Trisno. In search of a linear electro-optic amplitude modulator. *IEEE Photonics Technology Letters*, vol 3 no 2, pp 144+, February 1991.

[6] H. Skeie and R. V. Johnson. Linearization of electro-optic modulators by a cascade coupling of phase modulating electrodes. In *Integrated Optical Circuits*, no. 1583, pp 153-164. SPIE, SPIE, 1991

[7] J. F. Lam and G. L. Tangonan. A novel optical modulator system with enhanced linearization properties. *IEEE Photonics Technology Letters* vol 3 no. 12 pp 1102+, Dec 1991.

[8] S. K. Korotky and R. M. Ridder. Parallel modulation schemes for hwo distortion analog optical transmission. *IEEE Journal on Select Areas in Communications* vol 8 no. 7 pp 1377+, 1990.

[9] W. K. Burns. Linearized optical modulator with fifth order corrections. *Journal of Lightwave Technology,* vol 13 no. 8, 1995.

[10] Anders Djupsöbacka. A linearization concept for integrated-optic modulators. *IEEE Photonics Technology Letters* Vol 4 no 8, pp 869+, August 1992.

[11] L. M. Johnson and H.V. Roussell. Reduction of intermodulation distortion in interferometric optical modulators. *Optics Letters*, vol 13 no. 10 pp 928+, 1988.

[12] L. M. Johnson and H.V. Roussell. Linearization of an interferometric modulator at microwave frequencies by polarization mixing. . *IEEE Photonics Technology Letters.* vol 2 no. 11, pp 810+, November 1990.

[13] R. B. Childs and V. A. O'Byrne. Pre-distortion Linearization of directly modulated DFB lasers and external modulators for AM video transmission. *In Optical Fiber Communications Conference*, Technical Digest Vol1, Paper WH6, OSA/IEEE, San Francisco.

[14] R. G. Hunsperger. *Integrated Optics: Theory and Technology.* 3rd Edition, Spinger-Verlag, New York 1991.

[15] H. Haus. *Waves and Fields in Opto-electronics.* Prentice Hall, Englewood Cliffs, New Jersey, 1984.

[16] T. Tamir, Ed. *Guided-Wave Optoelectronics.* 2nd Edition Springer-Verlag, New York, 1990

[17] R. Marcuse. *Theory of Dielelectric Optical Waveguides.* Academic Press, New York, 1974.

[18] H. Kogelnik, V. Ramaswamy. Scaling rules for thin film optical waveguides. *Applied Optics,* vol 13 no 8, August 1974.

[19] W. K. Burns. Normal mode analysis of waveguide devices. Part I: theory. *Journal of Lightwave Theory,* vol 6 no. 6 pp 1051+. June 1988

[20] A. Hardy and W. Streifer. Coupled-mode theory of parallel waveguides. *Journal of Lightwave Technology,* LT-3, pp 1135+, 1985.

[21] E. A. J. Marcatili. Improved coupled-mode equations for dielectric guides. *IEEE Journal of Quantum Electronics.* vol QE-22, pp 988+, 1986.

[22] B. E. Little, C. Wu, W. P. Huang. Synthesis of codirectional couplers with ultralow sidelobes and minimum bandwidth, *Optics Letters,* vol. 20, p. 1259, 1995.

[23] B. E. Little. Ideal wavelength filters using semi-adiabatic coupling. *Optics Letters.* vol. 21, p. 1424, 1996.

[24] Lowell B. Koppel. *Introduction to Control Theory with Applications to Process Control.* Prentice Hall, Englewood Cliffs, New Jersey, 1968.